



# **JGR** Solid Earth

# RESEARCH ARTICLE

10.1029/2021JB022715

# **Special Section:**

Ophiolites and Oceanic Lithosphere, with a focus on the Samail ophiolite in Oman

#### **Key Points:**

- Sm-Nd garnet, U-Pb zircon, and U-Pb rutile dates from As Sifah cluster from ~81-77 Ma
- All data suggest NE-dipping subduction of the Arabian continental margin beneath the already-obducted Samail Ophiolite
- Deep subduction of the Arabian margin occurred similarly to other small HP bodies, followed by twostage (rapid then slow) exhumation

### **Supporting Information:**

Supporting Information may be found in the online version of this article.

### Correspondence to:

J. M. Garber, jxg1395@psu.edu

## Citation:

Garber, J. M., Rioux, M., Searle, M. P., Kylander-Clark, A. R. C., Hacker, B. R., Vervoort, J. D., et al. (2021). Dating continental subduction beneath the Samail Ophiolite: Garnet, zircon, and rutile petrochronology of the As Sifah eclogites, NE Oman. *Journal of Geophysical Research: Solid Earth*, *126*, e2021JB022715. https://doi.org/10.1029/2021JB022715

Received 29 JUN 2021 Accepted 5 NOV 2021

## **Author Contributions:**

Conceptualization: Joshua M. Garber, Matthew Rioux, Michael P. Searle, Bradley R. Hacker Data curation: Joshua M. Garber, Matthew Rioux, Andrew R. C. Kylander-Clark, Jeff D. Vervoort Formal analysis: Joshua M. Garber, Matthew Rioux, Jeff D. Vervoort Funding acquisition: Joshua M. Garber, Matthew Rioux, Bradley R. Hacker

© 2021. American Geophysical Union. All Rights Reserved.

# Dating Continental Subduction Beneath the Samail Ophiolite: Garnet, Zircon, and Rutile Petrochronology of the As Sifah Eclogites, NE Oman

Joshua M. Garber<sup>1</sup>, Matthew Rioux<sup>2,3</sup>, Michael P. Searle<sup>4</sup>, Andrew R. C. Kylander-Clark<sup>2,3</sup>, Bradley R. Hacker<sup>2,3</sup>, Jeff D. Vervoort<sup>5</sup>, Clare J. Warren<sup>6</sup>, and Andrew J. Smye<sup>1</sup>

<sup>1</sup>Department of Geosciences, The Pennsylvania State University, University Park, PA, USA, <sup>2</sup>Department of Earth Science, University of California Santa Barbara, Santa Barbara, CA, USA, <sup>3</sup>Earth Research Institute, University of California Santa Barbara, CA, USA, <sup>4</sup>Department of Earth Sciences, Oxford University, Oxford, UK, <sup>5</sup>School of the Environment, Washington State University, Pullman, WA, USA, <sup>6</sup>School of Environment, Earth and Ecosystem Sciences, The Open University, Milton Keynes, UK

**Abstract** Studies of the high-pressure (HP) As Sifah eclogites in the NE Saih Hatat Window, Oman, have used different combinations of radiometric dating results (Ar/Ar, Sm-Nd vs. U-Pb, Rb-Sr) to interpret disparate tectonic models for the timing, geometry, and cause of continental subduction—including its relationship to the Samail Ophiolite. To determine the timing of continental subduction, we coupled petrochronological analyses of major (garnet) and accessory phases (zircon and rutile) from the highest grade metamorphic rocks (As Sifah eclogites) in the Saih Hatat. Early Permian (283.8 ± 0.7 Ma) tuffaceous zircon cores are consistent with earlier interpretations that the As Sifah rocks were sourced from a distal portion of the Arabian continental margin. Data from a range of bulk compositions and metamorphic assemblages consistently suggest a single metamorphic event with garnet growth from ~81 to 77 Ma—though with slight, consistent offsets in the timing of metamorphic (re)crystallization between different lithologies. These new data confirm previous interpretations for continental HP metamorphism in a single NE-dipping subduction zone beneath the obducted Samail Ophiolite; there is no robust evidence for an ~110 Ma event or for SWdipping subduction beneath the Arabian plate. Combined with other constraints, our data suggest that the As Sifah unit was subducted at rates similar to other small continental HP bodies, followed by two stages of cooling and exhumation—likely associated with the dragging to mantle depths by a mafic root, an initial phase of rapid exhumation from mantle depths, and a lengthy residence (≤40 My) in the lower to middle

Plain Language Summary The subduction of continental material to mantle depths is of interest because (a) it is associated with the recycling of surface material to the deep mantle and (b) these types of rocks have been exhumed to the Earth's surface almost exclusively since ca. 1.0 Ga. The Saih Hatat window, Oman, is a unique expression of this process where buoyant continental rocks were apparently subducted and exhumed beneath a denser ophiolite (slice of oceanic crust and mantle). However, the timing and geometry of this process has been controversial. We measured isotopic dates and trace elements from several different minerals in a suite of representative samples from the the highest-grade, eclogite-facies metamorphic rocks in the Saih Hatat, and found that each gave the same range of dates (~81–77 Ma). There are small variations due to changes in bulk composition, but the data firmly suggest a single subduction metamorphism episode. These results require the subduction of the Arabian continental margin after the obduction of the Samail Ophiolite, and suggest that the most deeply subducted, most outboard continental margin rocks were anchored to a dense mafic root before detaching, exhuming (first quickly, then more slowly), and eventually becoming exposed in tectonic windows through the ophiolite.

# 1. Introduction

High- to ultrahigh-pressure (*HP-UHP*) continental subduction is a well-documented process that appears to be a hallmark of plate tectonics at least since the Neoproterozoic. Exposed examples of continental subduction beneath continental upper plates show consistent trends in their rates of subduction and exhumation from the mantle, primarily based on their size, orogenic stage, and bulk composition (Kylander-Clark et al., 2012;

GARBER ET AL. 1 of 26



Investigation: Joshua M. Garber, Matthew Rioux, Michael P. Searle, Andrew R. C. Kylander-Clark, Clare J. Warren

Methodology: Joshua M. Garber, Matthew Rioux, Andrew R. C. Kylander-Clark, Bradley R. Hacker, Jeff D. Vervoort

**Project Administration:** Joshua M. Garber, Matthew Rioux, Bradley R. Hacker

Resources: Joshua M. Garber, Matthew Rioux, Michael P. Searle, Andrew R. C. Kylander-Clark, Bradley R. Hacker, Jeff D. Vervoort, Clare J. Warren, Andrew J. Smye

Supervision: Joshua M. Garber, Matthew Rioux, Michael P. Searle, Andrew R. C. Kylander-Clark, Bradley R. Hacker, Jeff D. Vervoort, Andrew J. Smye

Validation: Joshua M. Garber, Matthew Rioux, Michael P. Searle, Bradley R. Hacker, Jeff D. Vervoort, Clare J. Warren, Andrew J. Smye

**Visualization:** Joshua M. Garber, Matthew Rioux

**Writing – original draft:** Joshua M. Garber

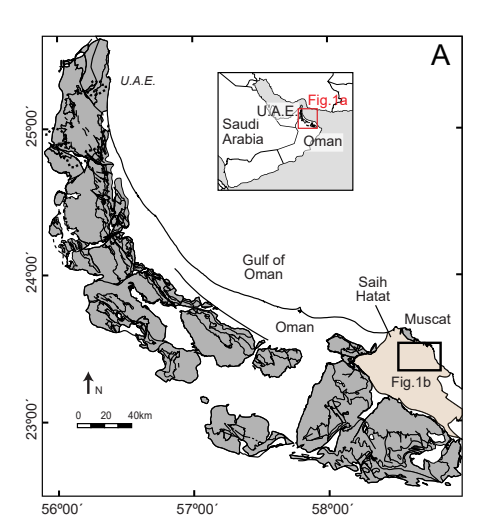
Writing – review & editing: Joshua M. Garber, Matthew Rioux, Michael P. Searle, Andrew R. C. Kylander-Clark, Bradley R. Hacker, Jeff D. Vervoort, Clare J. Warren Young & Kylander-Clark, 2015). In contrast, continental subduction beneath oceanic crust is rare and is typically observed in association with recent (<100 Ma) ophiolite obduction, including in New Caledonia and Oman (e.g., Agard & Vitale-Brovarone, 2013). This style of continental subduction occurs under some of the coldest modern metamorphic geotherms (Agard et al., 2018; Agard & Vitale-Brovarone, 2013; Vitale Brovarone & Agard, 2013), contrasting with the ultrahigh metamorphic temperatures ( $T = 800-900^{\circ}$ C) attained during sole metamorphism at the base of ophiolites that now structurally overlie these HP rocks (Agard et al., 2016; Cowan et al., 2014; Dewey & Casey, 2013; Hacker & Mosenfelder, 1996; Soret et al., 2017; Searle & Cox, 2002).

The northern part of the Saih Hatat Window of NE Oman (Figure 1) is the best exposed example of this type of HP continental orogen, but the sequence of tectonic events leading to continental subduction is controversial. Contrasting geochronology on the structurally lowest, highest grade metamorphic rocks in the Saih Hatat, at As Sifah beach  $(P > 2.0 \text{ GPa}, T > 530^{\circ}\text{C}$ : Massonne et al., 2013; Searle et al., 1994; Warren and Waters, 2006), has led to two entirely different interpretations for the timing and geometry of subduction. Based on Ar/Ar mica dates and Sm-Nd garnet-WR isochron dates (El-Shazly & Lanphere, 1992; Gray, Hand, et al., 2004; Gray, Miller, et al., 2004; Goscombe et al., 2020; Miller et al., 1999; Montigny et al., 1988) as well as structural arguments (Gray, Hand, et al., 2004; Gray, Miller, et al., 2004; Miller et al., 1998; Miller et al., 2002), one model suggests that the deeply subducted As Sifah rocks are polymetamorphic, with a prograde metamorphic episode around ~130-110 Ma and exhumation-related metamorphism at ~80 Ma. This model has also been suggested in the context of continental subduction to the SW, that is, toward the Arabian margin (e.g., Gregory et al., 1998; Gray & Gregory, 2000; Goscombe et al., 2020). A separate set of studies not only based on U-Pb zircon and Rb-Sr isochron dating (El-Shazly et al., 2001; Searle et al., 2004; Warren et al., 2003; Warren et al., 2005) but also supported by structural, metamorphic, and stratigraphic studies (El-Shazly et al., 1990; Goffé et al., 1988; Searle et al., 1994; Searle & Cox, 1999, 2002; Searle et al., 2004; Warren & Miller, 2007), suggests a single metamorphic episode for the As Sifah rocks at ~80 Ma during subduction to the NE away from the Arabian margin. Because this episode would immediately postdate and match the polarity of subduction beneath the Samail Ophiolite (Cowan et al., 2014; Rioux et al., 2016; Searle et al., 2004; Searle, 2007), this interpretation suggests that continental subduction arose as the last part of the same process driving ophiolite formation and obduction (a case numerically modeled by Duretz et al., 2016). In this case, all older Ar/Ar and Sm-Nd dates must be erroneous. This is not particularly controversial for the Ar/Ar dates, because extraneous Ar has been repeatedly shown to be a problem in HP metamorphic rocks in general and the As Sifah eclogites in particular (El-Shazly et al., 2001; Smye et al., 2013; Warren et al., 2011). Likewise, Sm-Nd dates can be affected by LREE-rich inclusions in garnet (e.g., Scherer et al., 2000), and the accuracy of the As Sifah Sm-Nd dates has been questioned by other authors (e.g., Warren et al., 2005).

There is little dispute that the uppermost, low-grade blueschist-facies continental nappes in the Saih Hatat region preserve only a single-stage metamorphic history related to ophiolite obduction onto the margin at ~80 Ma (e.g., El-Shazly & Lanphere, 1992). Additionally, different authors have used the same structural and metamorphic observations from the deeper, high-grade portions of the Saih Hatat Window in support of either a single-stage (El-Shazly et al., 1990; Searle et al., 2004; Warren & Miller, 2007) or polymetamorphic history (Gray, Hand, et al., 2004; Gray, Miller, et al., 2004; Goscombe et al., 2020; Miller et al., 1999). For example, proponents of the ~130-110 Ma subduction model have cited polyphase shear-sense indicators and outcrop- to regional-scale asymmetric folds, as well as variable garnet inclusion textures, as evidence for two distinct tectonic events separated by tens of My (Gray, Hand, et al., 2004; Gray, Miller et al., 2004). In contrast, proponents of the younger ~80 Ma subduction model argue that these different folding and shearing episodes could have been attained in different structural stages of the same tectonic event (i.e., subduction and exhumation) (e.g., Searle et al., 2004). The controversy thus hinges entirely on the timing and duration of metamorphism in the lowermost rocks, particularly how Sm-Nd and U-Pb dates relate to the growth of rock-forming metamorphic phases. Therefore, to understand the timing of metamorphism in the most deeply subducted rocks in the Saih Hatat, we performed new high-resolution garnet, zircon, and rutile isotopic (Sm-Nd and U-Pb) and trace-element measurements on the As Sifah eclogites. These data provide robust new constraints on the timing of subduction metamorphism and the protolith character of the subducted rocks; they also provide a unique comparison between the metamorphic, isotopic, and geochemical records in different end-member bulk compositions during the same event. We conclude

GARBER ET AL. 2 of 26





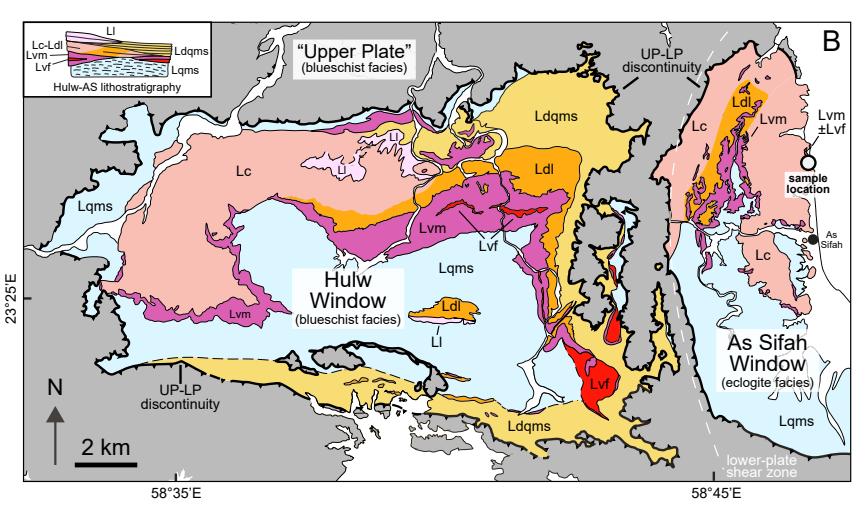


Figure 1. (a) Regional overview map modified from Nicolas et al. (2000) showing the Samail ophiolite (dark gray) and subducted continental margin rocks of the Saih Hatat (light brown). (b) Lithologic map of the Hulw and As Sifah Windows in the Saih Hatat, modified from Miller et al. (2002), Searle et al. (2004), and Warren and Miller (2007). The dominant structural feature is the "UP-LP" discontinuity (bold line), which separates "Upper Plate" rocks (dark gray) from "Lower Plate" units. A poorly exposed but structurally necessary ductile shear zone between the Hulw and As Sifah Windows is shown in a dashed white line. Unit abbreviations: Lqms, lower-plate quartz-mica schist; Lvf, lower-plate felsic volcanic; Lvm, lower-plate mafic volcanic; Lc, lower-plate calcschist and quartz schist; Ldl, brown dolomite; Ldqms, dolomitic quartz-mica schist; Ll, Permian metacarbonate. The inset stratigraphic sketch is modified from Miller et al. (2002); these "Lower-Plate" units in the Hulw and As Sifah Windows are interpreted as stratigraphically correlative equivalents of the Ordovician (Lqms; Amdeh Fm.) to Permian (Lc-Ll; Saiq Fm.) Arabian continental margin sequence that is also exposed in the "Upper Plate" (e.g., Searle et al., 2004; Warren & Miller, 2007).

by comparing our data to other (U)HP orogens globally to understand the unique tectonic character of continental subduction beneath ophiolites.

# 2. Geologic Background

The Saih Hatat Window (NE Oman) records the partial subduction and exhumation of the Arabian continental margin (Agard et al., 2010; Duretz et al., 2016; El-Shazly et al., 1990; El-Shazly et al., 2001; El-Shazly & Coleman, 1990; El-Shazly & Lanphere, 1992; Gregory et al., 1998; Gray, Hand, et al., 2004; Gray, Miller, et al., 2004; Goffé et al., 1988; Jolivet et al., 1998; Lippard, 1983; Le Metour et al., 1986; Le Métour et al., 1990; Michard, 1983; Michard et al., 1991; Michard et al., 1994; Searle, 2007; Searle et al., 1994; Searle et al., 2004; Warren et al., 2003; Warren et al., 2005; Warren & Miller, 2007; Yamato et al., 2007). This record is expressed as a domed series of stacked, metamorphosed (high-P/low-T), fault- or shear-zone-bounded units exposed in a structural window through the obducted Samail Ophiolite (Figure 1a). The stratigraphy of most of the Saih Hatat, including that of the Hulw and As Sifah Windows (below), is correlative to the Precambrian to Cretaceous continental margin sequence exposed elsewhere in the Oman Mountains including the Jebel Akhdar Window to the west (e.g., Chauvet et al., 2009; Glennie et al., 1973; Mann & Hanna, 1990), permitting detailed structural reconstructions (Miller et al., 2002; Searle et al., 2004; Warren & Miller, 2007). The rocks are multiply deformed, but the primary penetrative structural features are top-to-the-NNE fabrics related to the exhumation of footwall rocks to the southwest (Agard et al., 2010; Searle et al., 1994, 2004), which is associated with the timing of peak to retrograde metamorphism (El-Shazly et al., 1990; El-Shazly et al., 1997; Warren et al., 2003).

The most deeply subducted rocks in the Saih Hatat (Figure 1b) occur in two exposures beneath a major shear zone that has been termed the Upper Plate-Lower Plate (UP-LP) discontinuity (Gregory et al., 1998; Miller et al., 1998; Miller et al., 2002) or the Hulw Detachment (Searle et al., 2004, 2005), although similar P-T conditions from multi-equilibrium thermobarometry above and below the structure suggest that this shear zone is probably not a lithosphere-scale feature (Agard et al., 2010; Gray, Gregory, & Miller, 2005; Searle et al., 2004; Searle et al., 2005; Yamato et al., 2007). In the westernmost exposure (Hulw Window), the UP-LP discontinuity separates rocks that show a similar peak metamorphic P above and below the detachment ( $\sim$ 1.0 GPa) and a little variation in T, either across the discontinuity or within the window itself (Agard et al., 2010; Yamato et al., 2007;

GARBER ET AL. 3 of 26



although see El-Shazly, 2001 for a consideration of lower peak metamorphic P for rocks in the Hulw Window [ $\sim$ 6.5–8.5 kbar]). However, there is a major increase in deformation intensity toward the shear zone in the upper plate (Miller et al., 2002). The easternmost As Sifah Window exhibits a stratigraphic sequence matching the Hulw Window (Figure 1b, inset) (Miller et al., 2002; Warren & Miller, 2007), but with significantly higher peak metamorphic pressures and temperatures ( $P \ge 2.0$  GPa, T = 550–600°C) (Massonne et al., 2013; Searle et al., 1994; Warren and Waters, 2006; Yamato et al., 2007). Unlike the Hulw Window, the As Sifah Window shows an apparent increase in metamorphic grade to the NNE (Searle et al., 2004; Yamato et al., 2007), although this may also reflect different extents of retrogression (Warren and Waters, 2006). Highly attenuated isoclinal folds in both windows are cut by the UP-LP discontinuity, suggesting that the As Sifah rocks were exhumed to the same depth as the Hulw Window prior to mostly lateral motion along the shear zone (Gray, Miller, et al., 2004; Miller et al., 2002; Searle et al., 2004; Warren & Miller, 2007).

The structurally lowest, highest grade metamorphic rocks in the Saih Hatat are exposed in metavolcanic lenses along the coast ~1-2 km north of the village of As Sifah (Figure 1b). The lithologic horizon in which the highest grade assemblages occur is recognizable and traceable through the entirety of the Hulw and As Sifah Windows (units Lym and Lyf on Figure 1b: Chauvet et al., 2009; Gray, Gregory, Armstrong, et al., 2005; Miller et al., 2002; Warren & Miller, 2007), but they only contain eclogite-facies assemblages within a few km of coast (Searle et al., 1994; Searle et al., 2004; Warren and Waters, 2006). A SHRIMP U-Pb zircon date from a felsic metatuff at As Sifah suggested that this horizon represents late Carboniferous (~298 Ma) volcanic flows and tuffs associated with the breakup of Pangaea (Gray, Gregory, Armstrong, et al., 2005), which is slightly older than the timing of extension recorded elsewhere in Oman (Angiolini et al., 2003). Still, this date fits within other "lower-plate" stratigraphic constraints: quartz-mica schists underlying the boudins have been correlated with the Ordovician Amdeh Formation, whereas calc-schists above (but still within the As Sifah Window) may represent the Permian Saiq Formation (Miller et al., 2002; Searle et al., 2004; Warren & Miller, 2007), suggesting that the As Sifah beach exposure represents an outboard subducted remnant of the pre-Permian unconformity observed throughout NE Oman. Most workers thus conclude that the As Sifah and Hulw Windows reflect a more distal, deeper water, and more siliciclastic part of the same Arabian margin sequence exposed in stratigraphically correlative, structurally higher, but lower grade units (Chauvet et al., 2009; Searle et al., 2004; Warren & Miller, 2007), while others have suggested they are the remnants of an outboard microplate (Gray, Gregory, Armstrong, et al., 2005; Gray & Gregory, 2000; Gray, Miller, et al., 2004).

Our sampling location (As Sifah beach; see Figure 1b) is described in detail elsewhere, including Searle et al. (2004), their Figure 7 and Gray, Miller, et al. (2004), their Figure 7. The outcrop is a lens of foliated to granoblastic mafic garnet blueschists and eclogites with less common (but still eclogite-facies) schistose felsic layers; this mafic lens is enclosed by metacarbonates and calcschists and crosscut by quartz-carbonate-hematite veins (El-Shazly et al., 1990; El-Shazly et al., 1997; El-Shazly, 2001; Gray, Gregory, Armstrong, et al., 2005; Gray, Hand, et al., 2004; Gray, Miller, et al., 2004; Searle et al., 1994; Searle et al., 2004; Warren and Waters, 2006; Massonne et al., 2013). Several lines of evidence, including garnet-clinopyroxene-phengite thermobarometry (Searle et al., 1994), P-T pseudosections with solution models amended to account for the presence of significant Fe<sup>3+</sup> (Warren and Waters, 2006), Si-in-phengite barometry (Massonne et al., 2013), and the presence of radial cracks around quartz inclusions in garnet (Wendt et al., 1993), suggest peak P-T conditions of ~2.0-2.5 GPa and ~550°C. In contrast, El-Shazly (2001) used several well-characterized thermobarometers coupled to phase relations, end-member petrogenetic grids, and comparisons to other well-studied high-P metamorphic terranes to argue for significantly lower pressures in the As Sifah eclogites (<1.6 GPa). El-Shazly (2001) further noted that phengite was not in equilibrium with the peak garnet-clinopyroxene assemblage in the mafic rocks and argued that the absence of high-P phases in interleaved felsic assemblages was inconsistent with any of the As Sifah rocks reaching the higher pressures determined in other studies. However, Warren and Waters (2006) argued that albite-magnetite aggregates in these felsic rocks represent pseudomorphs after clinopyroxene, and similar felsic rocks studied here (Section 3, below) contain garnet, rutile, and Si-rich phengite in the peak assemblage (Massonne et al., 2013)—all of which are consistent with the higher P estimates. All rocks reached peak conditions along clockwise P-T paths and relatively cold geotherms (El-Shazly et al., 1990; El-Shazly & Coleman, 1990) that are variably recorded by different bulk compositions (El-Shazly et al., 1997). Some rocks contain relict prograde

GARBER ET AL. 4 of 26



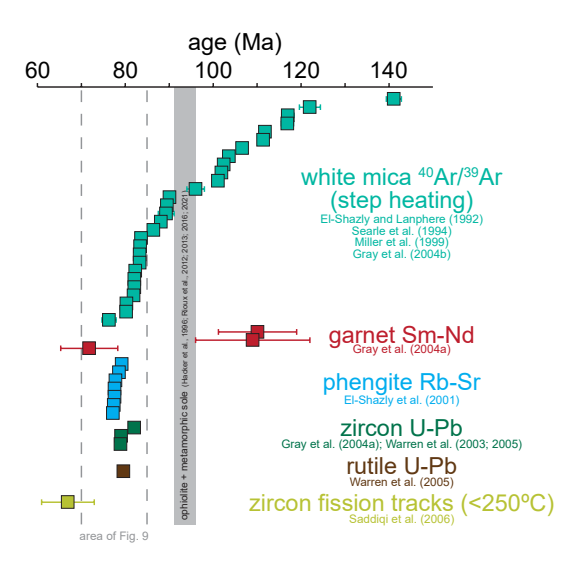


**Figure 2.** Previous geochronology from the As Sifah eclogites. Where not visible, error bars on dates are smaller than symbols. The existence of a  $\sim$ 110 Ma metamorphic event at As Sifah has been postulated based on two Sm-Nd garnet-WR isochron dates and an array of old white-mica  $^{40}$ Ar/ $^{39}$ Ar step-heating dates, whereas U-Pb and Rb-Sr isotopic data consistently give young,  $\sim$ 80 Ma dates. See text for additional discussion.

minerals as inclusions in garnet cores (including lawsonite pseudomorphs and chloritoid), whereas other rocks contain garnets with only peak to early retrograde metamorphic phases such as rutile, phengite, blue amphibole, and omphacite-, aegirine-, and/or jadeite-rich pyroxene (El-Shazly et al., 1997; El-Shazly, 2001; El-Shazly & Liou, 1991; Gray, Hand, et al., 2004; Gray, Miller, et al., 2004; Massonne et al., 2013; Warren and Waters, 2006). Most mafic rocks, particularly those that suffered fluid ingress (El-Shazly et al., 1997), have been affected by a late retrograde overprint to an epidote-albite-green amphibole-chlorite assemblage, suggesting slight heating during retrogression (e.g., El-Shazly et al., 1990; Gray, Miller, et al., 2004; Massonne et al., 2013). There is no existing mineralogical or garnet chemical zoning evidence for distinct metamorphic stages nor for a pause between different garnet growth episodes (e.g., Warren and Waters, 2006).

As noted above, there is a long and controversial history of geochronology from the As Sifah rocks (Figure 2). On the basis of K-Ar white mica ages spanning  $\sim$ 130–80 Ma in the Hulw and As Sifah Windows as well as  $^{40}$ Ar/ $^{39}$ Ar step heating experiments, Montigny et al. (1988) reasoned that the HP metamorphic history of As Sifah could have involved (a) two distinct metamorphic events, one at  $\sim$ 130–110 Ma and the other at  $\sim$ 80 Ma, or (b) a single metamorphic episode at  $\sim$ 80 Ma with older dates resulting from extraneous Ar. A similar conclusion (distinct  $\sim$ 110 and 80 Ma HP metamorphic episodes) was reached by El-Shazly and Lanphere (1992) based on additional  $^{40}$ Ar/ $^{39}$ Ar data; however, subsequent Rb-Sr isochron dating led the

same group to interpret that all older  $^{40}$ Ar/ $^{39}$ Ar dates result from extraneous Ar and all metamorphism occurred solely at  $\sim$ 80 Ma (El-Shazly et al., 2001). This contention was subsequently strengthened by TIMS U-Pb zircon and rutile ages of  $\sim$ 79–78 Ma (Warren et al., 2003; Warren et al., 2005), each of which occurs as inclusions in the major rock-forming phases—suggesting peak metamorphism at that time.

In contrast, Gray, Hand, et al. (2004) dated eclogite-facies assemblages in the As Sifah Window to  $110 \pm 9$  Ma and  $109 \pm 13$  Ma using Sm-Nd garnet-whole rock (WR) isochrons and suggested that these represented the timing of peak HP metamorphism; a younger SHRIMP U-Pb zircon date at ~82 Ma (as well as other U-Pb and Rb-Sr dates, and a secondary Sm-Nd isochron date) was suggested to record exhumation. Further  $^{40}$ Ar/ $^{39}$ Ar dating of different generations of white micas (Miller et al., 1999; Gray, Miller, et al., 2004) in combination with detailed structural mapping (Miller et al., 1998; Miller et al., 2002) was used to suggest that As Sifah underwent prograde southward subduction at ~120–110 Ma and retrograde exhumation at ~80 Ma (Miller et al., 1998; Miller et al., 1999; Miller et al., 2002; Gray, Miller, et al., 2004). High-precision laser  $^{40}$ Ar/ $^{39}$ Ar dating of individual micas has since shown that extraneous Ar is significant in almost all As Sifah white micas, particularly in mafic rocks (Smye et al., 2013; Warren et al., 2011), firmly indicating that only the youngest published Ar/Ar dates (~80 Ma) are geologically meaningful. Still, the ~110 Ma Sm-Nd garnet dates from Gray, Hand, et al. (2004) continue to be cited in favor of continent-ward subduction during the Early Cretaceous (e.g., Goscombe et al., 2020).

# 3. Sample Descriptions

To understand the timing of (U)HP metamorphism as well as the pre- and syn-metamorphic history of rock protoliths, we sampled several different eclogite-facies rocks that reflect the textural/chemical diversity and range of metamorphic histories recorded at As Sifah. The descriptions below are focused on samples dated by the Sm-Nd method with subordinate descriptions for those without garnet dates. The approximate (visually estimated) modal mineralogy for each sample is shown in Table 1, and thin-section scans of each sample can be found online at doi: 10.17605/OSF.IO/CZG3P.

Sample CWO237 (23°27'30"N, 58°46'48"E) is a banded, foliated mafic eclogite, with layering defined by garnet-rich layers (1–2 mm diameter grains) with coarse-grained phengite, clinopyroxene, blue amphibole, epidote,

GARBER ET AL. 5 of 26



Table 1 Approximate Modal Mineralogy for the Studied Samples									
Sample	Description	Grt	Cpx	Gln	Ph	Qz	Ep	Rt	
CWO237	Foliated mafic eclogite	5	35	20	25		15	~1	
9125M02	Foliated mafic eclogite	5	35	25	5		30	~1	
CWO21	Foliated mafic eclogite	5	55	20	10	5	5	~1	
9125M04	Granoblastic mafic eclogite	15	35	30	5	15	tr	tr	
CWO23	Granoblastic mafic eclogite	20	15	15	15	35	tr	tr	
131219J02	Eclogite-facies metapelite	5			50	45		tr	

rutile, and hematite/ilmenite, alternating with garnet-absent, finer grained layers of the same phases. Garnet, clinopyroxene, and rutile are the texturally oldest phases in the sample; garnet grains are littered with fine inclusions of clinopyroxene and larger grains of rutile + opaques, with no gradation in inclusion assemblage from core to rim (Figures 3a and 3b). Garnet grains (and mm-scale clinopyroxene aggregates) are locally replaced by  $\sim 100-200-\mu$ m-thick rims and filled cracks with an assemblage of phengite, optically zoned blue amphibole, and epidote; the outline of these rims locally pseudomorphs the partially resorbed garnet grains (Figure 3c). Both coarse- and fine-grained layers contain abundant texturally late epidote that overprints most other phases in the sample. All phases are locally overprinted by chlorite  $\pm$  green amphibole, especially along garnet rims and cracks. Rare mm-scale carbonate clots (with biotite, green amphibole, and titanite-rimmed rutile) are distributed throughout the sample (Figure 3d).

Sample 9125M04 (23°27'19"N, 58°46'46"E) is a granoblastic mafic eclogite that is significantly coarser grained than CWO237 (garnet and blue amphibole grains up to ~0.5 cm in diameter) and contains quartz in the peak assemblage. Garnets in this sample exhibit darker pink cores in plane-polarized light that contain rare chloritoid and epidote but abundant quartz and opaque inclusions, grading to lighter pink rims with similar fine-grained clinopyroxene and rutile inclusions as in foliated eclogite CWO237 (Figure 3e). Garnet cores display an internal schistosity (defined primarily by opaques) that is typically at an angle to the external compositional foliation (Figure 3e). Blue amphiboles display striking optical zoning and contain numerous rutile inclusions (Figure 3f). This sample is significantly less retrogressed than CWO237, with chlorite and green amphibole limited to cracks in garnet; other phases were mostly unaffected.

Because we did not find zircon in either CWO237 or 9125M04, we analyzed zircon and rutile in an additional foliated mafic eclogite (CWO21; 23°27'30"N, 58°46'48"E) as well as rutile in another foliated (9125M02; 23°27'32"N, 58° 46'48"E) and granoblastic eclogite (CWO23; 23°27'30"N, 58°46'48"E). CWO21 and CWO23 have been described and dated by ID-TIMS U-Pb zircon and rutile techniques elsewhere (Warren et al., 2003; Warren et al., 2005). These other eclogite samples contain similar peak assemblages and textures as CWO237 and 9125M04, albeit with slightly different mineral compositions and proportions (Table 1); among all eclogite samples, CWO21, 9125M04, and CWO23 contain quartz (in order of increasing quartz mode), whereas CWO237 and 9125M02 do not. Where present, zircon and rutile in all samples are found as inclusions in all major phases, including within the texturally oldest garnet-clinopyroxene assemblages (see also Warren et al., 2003, their Figure 2).

Sample 131219J02 (23°27'13"N, 58°46'47"E) is a quartz-phengite-garnet-hematite-rutile-ilmenite felsic schist (originally classified as tuffaceous by Le Metour et al. (1986), and henceforth referred to as a "metafelsite") taken from a decameter-scale horizon at outcrop. This sample is broadly similar to the one studied by Massonne et al. (2013) but contains no peak metamorphic ferromagnesian silicates other than garnet. About 1–2-mm-sized garnet grains contain inclusions of quartz, rutile, hematite, ilmenite, and sulfide minerals and are highly retrogressed along chlorite and phengite-filled fractures that are texturally discordant to the phengite-defined foliation (Figure 3g). The sample contains abundant accessory apatite, rutile, and zircon; apatite occurs as 0.5–1.0 mm matrix grains, whereas <200-µm-long rutile and zircon grains are dominantly found as inclusions in phengite and quartz (Figure 3h) and only rarely in garnet. The sample also contains a scarce, texturally late, birefringent phase that is locally present along quartz grain boundaries, which was not chemically analyzed but is most likely barite (Massonne et al., 2013).

GARBER ET AL. 6 of 26

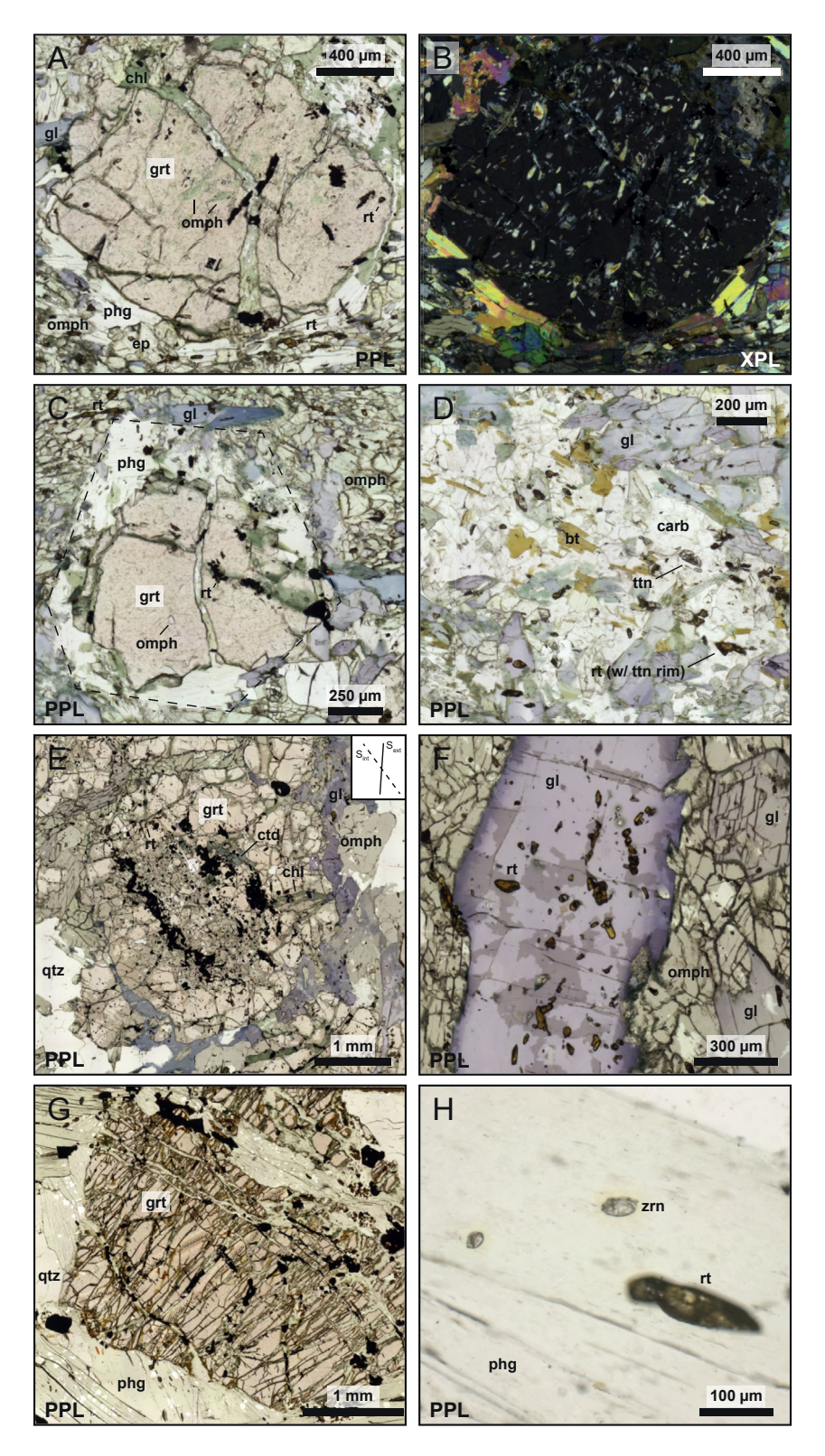


Figure 3.

GARBER ET AL. 7 of 26



# 4. Methods

Method details are documented in Text S1 in the Supporting Information S1 and are briefly outlined here. Garnet X-ray maps and major-element quantitative analyses were obtained by electron-probe microanalysis (EPMA) at the University of California, Santa Barbara (Figure S1 in Supporting Information S1, Table S1). Laser-ablation inductively coupled mass spectrometry (LA-ICPMS) trace-element measurements in garnet were also done at UCSB to supplement the interpretation of garnet geochronology (Table S2). Sm-Nd garnet-WR dating (Table 2) was performed on bulk garnet, whole-rock, and glaucophane aliquots from three samples by isotope-dilution mass spectrometry at the Washington State University Radiogenic Isotope and Geochronology Laboratory (RIGL) using the methods outlined in Johnson et al. (2018). Zircons were imaged by cathodoluminescence (CL) using an FEI Quanta 400f field-emission scanning electron microscope (FE-SEM) at UCSB. Laser-ablation split-stream zircon U-Pb and trace-element depth profiling (Table S3) and spot analyses (Table S4), as well as rutile U-Pb and trace-element spot analyses (Table S5), were performed at UCSB following the methods of Kylander-Clark et al. (2013). All U-Pb dates in the results section are reported with  $\pm 2\sigma$  internal uncertainties, but are displayed in Figure 9 with both  $\pm 2\sigma$  internal and  $\pm 2\sigma$  external uncertainties.

# 5. Results

# 5.1. Garnet EPMA Maps, Major-Element Transects, and Trace-Element Data

Garnet grains from all samples exhibit smooth, continuous core-to-rim Mg, Mn, and Fe zoning (Figure 4, top) with some diffusive Mg-rich haloes around inclusions (particularly in granoblastic eclogite 9125M04). Ca zoning is sharper and more complex in all garnets (Figure S1 in Supporting Information S1) and typically outlines earlier euhedral to subhedral cores. Garnets in all samples are dominated by almandine (~2.0–2.5 Fe apfu) and display similar, long-wavelength, oscillatory Fe profiles (Figure 4). Despite the differences between garnet inclusion assemblages in the granoblastic eclogite (91250M04) versus the foliated eclogite (CWO237), these samples broadly exhibit similar major-element zoning profiles. Garnet zoning in metafelsite 131219J02 is unremarkable other than the presence of thin, high-Ca rims (Figure 4).

The LA-ICPMS trace-element profiles are more complex and unique to each sample. Sm and Lu profiles are shown at the bottom of Figure 4 to demonstrate the relative behaviors of L-MREE and HREE, respectively, with the full REE patterns shown in the inset CI-normalized plots. Foliated eclogite CWO237 exhibits MREE decreases from garnet cores to rims, while HREE concentrations remain more consistent, although all REE concentrations are uniformly low (<2 ppm). Garnet grains in granoblastic eclogite 9125M04 show smoothly decreasing HREE and increasing L-MREE from core to rim, evocative of Rayleigh fractionation patterns described for trace-element uptake under similar (eclogite-facies) metamorphic conditions (Lapen et al., 2003). Metafelsite 131219J02 exhibits the most complex zoning, with HREE-poor garnet cores grading to HREE-rich, LREE-poor annuli, while the thin, calcic rims exhibit significant enrichments in all REE. To understand the significance of the Sm-Nd dates relative to garnet growth histories for each sample, we calculated the distribution of Sm along several core-to-rim garnet transects (Figure 5). Data for sample CWO237 were pooled into a single profile due to the small garnet grain size and number of data. These distributions show that granoblastic eclogite 9124M04 has the most "rim-biased" Sm concentrations, whereas the other samples contain a greater proportion of Sm in their cores; still, all analyzed garnets contain a majority of their Sm in the outer 20%–30% garnet radius, while at most

Figure 3. Rock and mineral textures from foliated, quartz-free eclogite CWO237 (a–d), granoblastic eclogite 9125M04 (e, f), and metafelsite 131219J02 (g, h). All photomicrographs were taken on a Zeiss Axio Scan Z.1 at Penn State. Patchy shading in panel (e–h) is due to an incompletely removed carbon coat. (a, b) Garnet porphyroblast in plane-polarized light (PPL) (a) and cross-polarized light (XPL) (b) from foliated eclogite CWO237, showing the partial replacement of the primary, dry, garnet-clinopyroxene-rutile assemblage by a hydrated phengite-epidote-glaucophane paragenesis. A second chlorite + green amphibole, greenschist-facies overprint is highly localized. Inclusions in all garnets from this sample are dominated by clinopyroxene + rutile. (c) Pseudomorphic replacement of garnet rims in CWO237 by phengite + glaucophane. (d) Rare carbonate "clot" in CWO237, containing biotite, green amphibole, and titanite-rimmed rutile. (e) Garnet porphyroblast from granoblastic eclogite 9125M04 with an internal schistosity defined by opaque minerals at an angle to the external foliation (see inset). These garnets contain prograde quartz, chloritoid, and epidote inclusions in their cores that grade to clinopyroxene + rutile at their rims. (f) Optically zoned blue amphibolite in 9125M04 (note darker blue rims and lighter blue cores) with numerous rutile inclusions. (g) Highly fractured garnet in metafelsite 131219J02 wrapped by matrix phengite + quartz. Note the laser ablation spots (although this is not the same garnet displayed in Figure 4). (h) Rutile and zircon grains included in matrix phengite from 131219J02 with radiation haloes around the zircon.

GARBER ET AL. 8 of 26



Table 2									
Sm-Nd Data	Summary From As Sifah I	Lithologies							
A 11	D 1.7	C ( )	NII/	1470 (1445) 1	2 (1)	14357 1714457 1	2 (1)	Dich	NT 1'e d

Aliquot	Description	Sm (ppm)	Nd (ppm)	<sup>147</sup> Sm/ <sup>144</sup> Nd	$2\sigma \text{ (abs)}^a$	<sup>143</sup> Nd/ <sup>144</sup> Nd	$2\sigma  (abs)^a$	Date <sup>b</sup>	$\epsilon Ndi^{c,d}$
CWO237	(foliated eclogite)								
G1 <sup>e</sup>	>710 µm garnet	0.85	0.81	0.632	0.003	0.513198	0.000040		
G2	355-710 µm garnet	0.76	0.50	0.924	0.005	0.513203	0.000036		
G3	180-355 μm garnet	0.65	0.15	2.580	0.013	0.514034	0.000033		
G4	180-355 μm garnet	0.64	0.16	2.467	0.012	0.513958	0.000058		
WR-B	bombed whole rock	3.34	11.49	0.176	0.001	0.512819	0.000027		
WR-S	tabletop whole rock	3.33	11.46	0.176	0.001	0.512801	0.000028		
								$77.5 \pm 2.2 \text{ Ma}$	$+3.8 \pm 0.4$
9125M04	(granoblastic eclogite)								
G1e	90–355 µm garnet	0.82	0.16	3.115	0.016	0.514246	0.000026		
G2	90–355 μm garnet	1.53	0.39	2.352	0.012	0.513727	0.000029		
G3	90–355 μm garnet	1.93	0.47	2.458	0.012	0.513778	0.000030		
G4	90-355 μm garnet	1.50	0.31	2.917	0.015	0.514050	0.000031		
G5e	90–355 μm garnet	1.22	0.44	1.688	0.008	0.513286	0.000032		
G6	90-355 μm garnet	1.65	0.61	1.633	0.008	0.513319	0.000028		
Glauc	355-710 µm glaucophane	1.14	6.25	0.110	0.001	0.512582	0.000027		
WR-B	bombed whole rock	1.86	2.95	0.382	0.002	0.512710	0.000033		
WR-S	tabletop whole rock	1.90	2.99	0.385	0.002	0.512718	0.000030		
								$79.0 \pm 3.2 \text{ Ma}$	$-0.3 \pm 0.7$
131219J02	? (metafelsite)								
G1	90–355 μm garnet	1.68	0.34	3.012	0.015	0.513817	0.000034		
G2	90-355 μm garnet	1.67	0.29	3.508	0.018	0.514066	0.000031		
G3	90–355 μm garnet	1.59	0.32	2.974	0.015	0.513772	0.000040		
WR-B1	Bombed whole rock	2.10	7.74	0.164	0.001	0.512300	0.000029		
WR-B2	Bombed whole rock	2.96	9.97	0.179	0.001	0.512304	0.000044		
WR-S1	Tabletop whole rock	3.02	10.16	0.180	0.001	0.512301	0.000028		
WR-S2	Tabletop whole rock	2.18	8.13	0.162	0.001	0.512301	0.000028		
								$80.9 \pm 1.3 \text{ Ma}$	$-6.2 \pm 0.3$

aln-run uncertainties only. bAge calculation includes propagated systematic uncertainties on all ratios. Calculated with CHUR parameters from Bouvier et al. (2008):  $^{143}$ Nd/ $^{144}$ Nd = 0.512630  $\pm$  0.000011,  $^{147}$ Sm/ $^{144}$ Nd = 0.1960  $\pm$  0.0004. dUncertainties include error on the calculated date and  $^{143}$ Nd/ $^{144}$ Nd<sub>i</sub>. Excluded from age calculation.

25% of the total Sm is contained in garnet cores. Therefore, Sm-Nd isochron dates are likely to be averages, albeit biased toward later increments of garnet growth in each sample.

We also performed LA-ICPMS trace-element transects in garnet from foliated mafic eclogite CWO21 (Figure S2 in Supporting Information S1) to compare with the zircon U-Pb and trace-element data collected from the same sample. The REE profiles are similar to those in granoblastic eclogite 9125M04 (Figure 4) with increasing L-MREE and decreasing HREE from core to rim.

# 5.2. Garnet-WR Sm-Nd Isotopic Data

Data for three samples are contained in Table 2 and displayed in Figure 6a. Out of a total twenty-two measured aliquots, three garnet aliquots in two samples plot significantly off their respective isochrons and are excluded as outliers. The remaining aliquots—including multiple garnet and whole-rock fractions for all samples, with an additional glaucophane aliquot in sample 9125M04—define three stacked isochrons, representing similar ages with

GARBER ET AL. 9 of 26



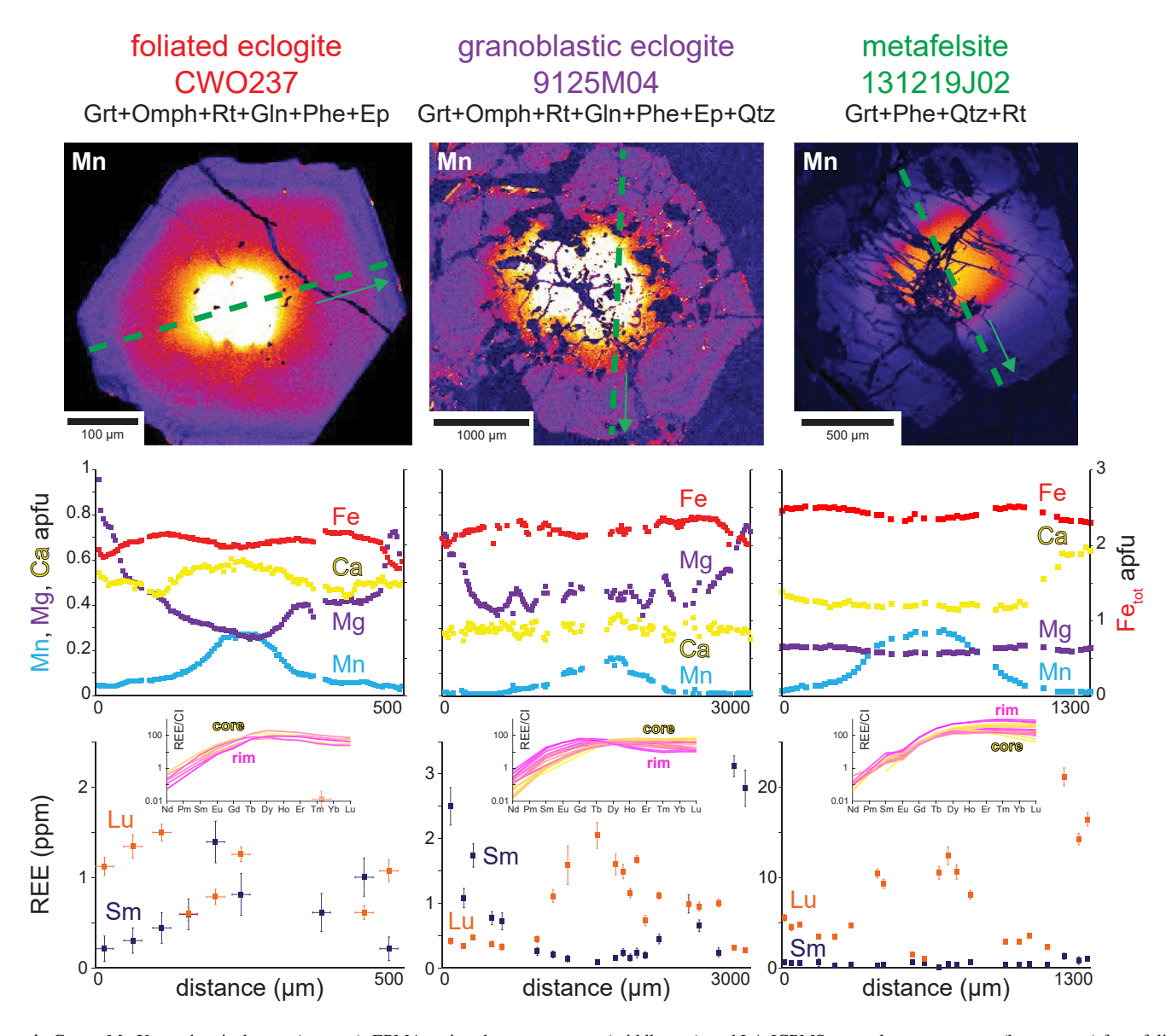
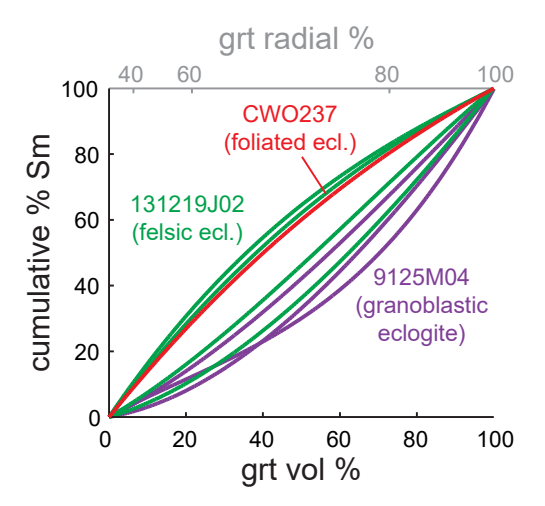


Figure 4. Garnet Mn X-ray chemical maps (top row), EPMA major-element transects (middle row), and LA-ICPMS trace-element transects (bottom row) from foliated eclogite CWO237 (left column), granoblastic eclogite 9125M04 (middle column), and metafelsite 131219J02 (right column). For the X-ray maps, warmer colors indicate higher concentrations (scaled individually to each garnet); Ca, Fe, and Mg maps for each garnet are displayed in Figure S1 in Supporting Information S1. The location of the quantitative transects—for both EPMA and LA-ICPMS data—is shown in green-dashed lines, with the arrow defining the left-to-right progression in the subsequent plots. The insets in the bottom row show CI-normalized (McDonough & Sun, 1995) REE data for each sample. All major- and trace-element data shown in this plot are contained in Tables S1 and S2.

different initial Nd isotope compositions. Foliated eclogite CWO237 yields the highest  $\varepsilon_{\rm Nd}(t)$  (+3.8 ± 0.4) and the youngest Sm-Nd isochron date (77.5 ± 2.2 Ma, n=5, MSWD = 0.53), in contrast to metafelsite 131219J02 with the lowest  $\varepsilon_{\rm Nd}(t)$  (-6.2 ± 0.3) and the oldest Sm-Nd isochron date (80.9 ± 1.3 Ma, n=7, MSWD = 0.23). These end-member Sm-Nd dates just overlap within their stated uncertainties, but an unpaired, two-tailed t-test establishes their difference at the 95% confidence interval (p < 0.007). Granoblastic eclogite 9125M04 is intermediate both isotopically ( $\varepsilon_{\rm Nd}(t) = -0.3 \pm 0.7$ ) and with respect to the calculated isochron date (79.0 ± 3.2 Ma, n=7, MSWD = 2.3). The average measured <sup>147</sup>Sm/<sup>144</sup>Nd ratio for garnet from each sample correlates with these age and whole-rock isotopic differences, with progressively increasing garnet <sup>147</sup>Sm/<sup>144</sup>Nd from foliated (youngest,  $+\varepsilon_{\rm Nd}$ ) to granoblastic to felsic eclogites (oldest,  $-\varepsilon_{\rm Nd}$ ) (Figure 6a). For each sample, both pressure-digested (bombed) and tabletop whole-rock aliquots plot in nearly identical places for each sample, suggesting that

GARBER ET AL. 10 of 26





**Figure 5.** Volume-normalized distribution of Sm for each LA-ICPMS garnet core-to-rim half-profile (9125M04 and 131219J02) or data from several compiled transects across small garnet grains (CWO237), including but not limited to the plots in Figure 4. Line colors match the lithologic classification in Figure 4. All trace-element data used to construct these plots are contained in Table S2.

there is little influence of inherited phases on the Sm-Nd isotopic results. Sm-Nd isotopic data from Gray, Hand, et al. (2004) are shown in Figure 6b for comparison; garnet <sup>147</sup>Sm/<sup>144</sup>Nd ratios are systematically lower than those determined in this study, and all points are bounded by the isotopic end-members defined by our new data.

# 5.3. Zircon U-Pb and Trace-Element Data

Multigrain zircon aliquots from foliated quartz-bearing eclogite CWO21 were previously dated by ID-TIMS U-Pb (Warren et al., 2003) with a concordia date of  $79.06 \pm 0.32$  Ma (n = 5, MSWD = 0.97). New CL images of these zircons show characteristic "soccer-ball" sector and fir-tree zoning (Figure 7a) similar to previous BSE images (Warren et al., 2003, their Figure 2c). Laser-ablation U-Pb spot data from this sample exhibit significant scatter along concordia and do not form a single population, with a lower intercept "errorchron" date of  $78.3 \pm 0.7$  Ma (n = 64, MSWD = 6.1); a weighted mean date excluding outliers yields a tighter uncertainty and better MSWD but an indistinguishable date ( $78.3 \pm 0.7$  Ma, MSWD = 2.5) (Figures 7b and 7c). Therefore, we quote the errorchron date and its uncertainty as an average age (discussed further below in Section 6.1.2). Trace-element abundances are extremely consistent across the entire zircon population; all grains lack a chondrite-normalized Eu anomaly and are depleted in HREE, but exhibit a Ce anomaly (Figure 7d). To understand

the metamorphic conditions at which these zircons (re)crystallized, we calculated Ti-in-zircon temperatures, which can be readily done for these grains because the presence of both quartz and rutile suggest unity  ${\rm TiO_2}$  and  ${\rm SiO_2}$  activities. With this assumption, the mean  $(1.95 \pm 0.22~{\rm ppm})$  or median  $(2.10~{\rm ppm})$  Ti concentrations from CWO21 zircon yield Ti-in-zircon temperatures (Ferry & Watson, 2007) of 612  $\pm$  27°C to 618  $\pm$  26°C (2 $\sigma$  external).

In contrast to the mafic zircons, the zircon images, depth profiles, and spot analyses from metafelsite 131219J02 show several age and trace-element populations. Zircon CL zoning is characterized by partly resorbed, CL-bright,

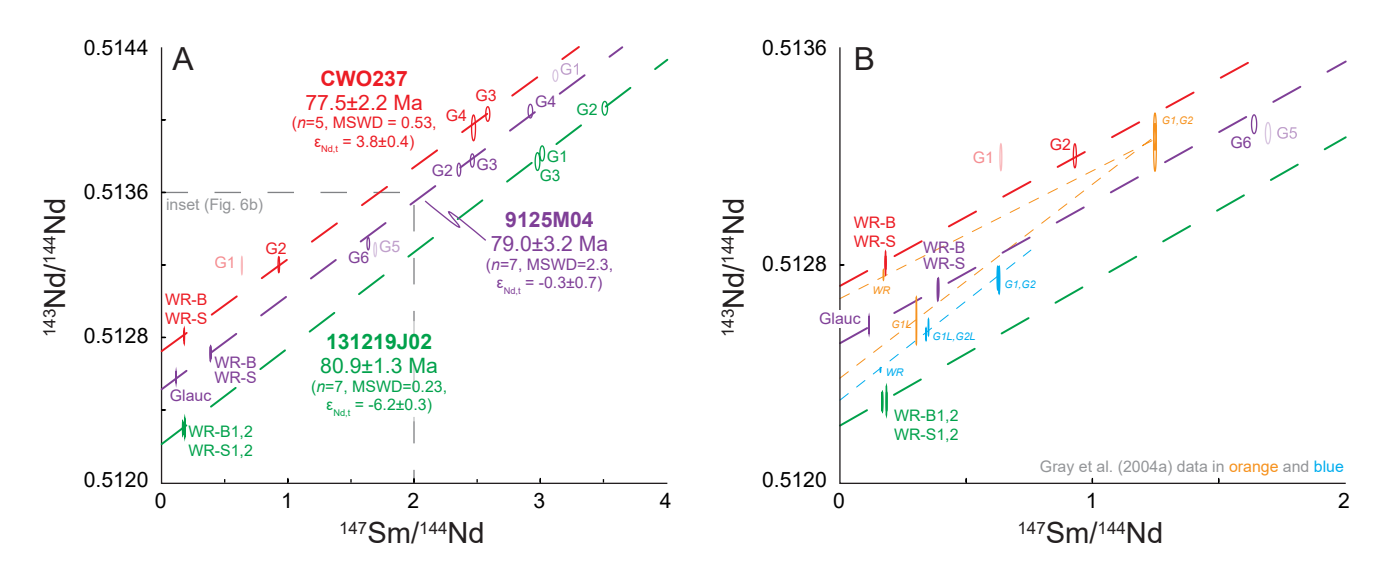


**Figure 6.** (a) Garnet-WR(-glaucophane) isochron data from this study (red, purple, and green colors as in Figures 4 and 5). Each sample in this study yields a broadly similar date defined by 5–7 data, but with clear differences in initial <sup>143</sup>Nd/<sup>144</sup>Nd. (b) Zoomed-in view of the lowest <sup>147</sup>Sm/<sup>144</sup>Nd data from this study, along with data from the same outcrop from Gray, Hand, et al. (2004) (orange and blue colors, with garnet, garnet leachate, and WR data). Note that (i) the garnet aliquots in this study plot at significantly higher average <sup>147</sup>Sm/<sup>144</sup>Nd and more precise <sup>143</sup>Nd/<sup>144</sup>Nd than in previous work, and that (ii) the steeper, apparently older "isochrons" from Gray, Hand, et al. (2004) connect data arrayed between the lithologic end-members defined here. All data used to construct these plots are contained in Table 2 and Gray, Hand, et al. (2004) (their Table 1).

GARBER ET AL. 11 of 26



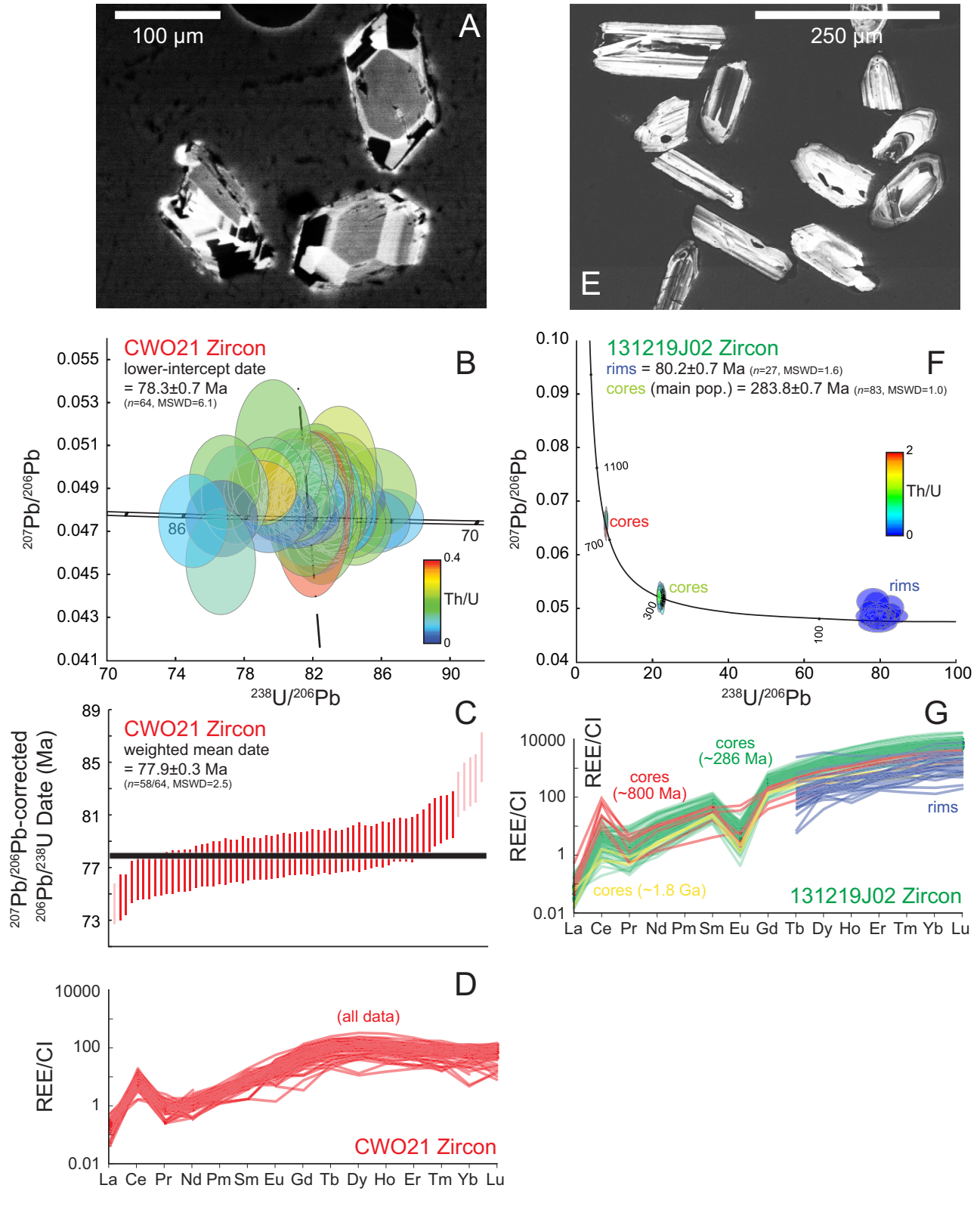


Figure 7.

GARBER ET AL. 12 of 26



oscillatory/concentrically zoned cores with thin ( $\leq 5 \mu m$ ) CL-dark zircon rims (Figure 7e). Depth profiles through the rims reveal a single age- and trace-element population at  $80.2 \pm 0.7$  Ma (n = 27, MSWD = 1.6) (Figure 7f) with the lowest Th/U ( $\sim 0.01$ ) and lowest total REE abundances in the sample. These rims exhibit a consistently positive CI-normalized REE slope from Dy to Lu in all rim analyses (Figure 7g); however, we did not measure Ti and L-MREE to determine Eu  $\pm$  Ce anomalies or Ti-in-zircon temperatures due to exceedingly low concentrations. Spot analyses on CL-bright cores—as well as depth profiles that penetrated through the younger rims—show a second age population at  $283.8 \pm 0.7$  Ma (n = 83, MSWD = 1.0) (Figure 7f), with higher Th/U (0.1-2), higher total REE, and consistently negative Eu/Eu\* and positive Ce/Ce\* (Figure 7g). Sparse older zircon cores (with  $\sim 80$  Ma rims) were also identified, including three grains with  $\sim 800$  Ma dates and a single grain with a concordant  $\sim 1.8$  Ga date (Figure 7f). These grains are not distinct in CL but they do exhibit unique trace-element characteristics. For example, the  $\sim 800$  Ma population displays the most extreme Ce anomalies, the most muted Eu/Eu\*, and the lowest P + Hf concentrations in the data set, while the  $\sim 1.8$  Ga grain displays the least extreme Ce anomalies (Figure 7g).

#### 5.4. Rutile U-Pb and Trace-Element Data

Rutile U-Pb dates and most trace elements vary as a function of bulk-rock lithology (Figure 8). For example, the U content of rutile progressively increases from foliated, quartz-free mafic eclogites (≤5 ppm) to the quartz-bearing foliated eclogite (5–10 ppm) to granoblastic eclogites (~10 ppm) to the end-member metafelsite (≤30 ppm), leading to progressively more precise U-Pb dates. On the other hand, while rutile grains are included in almost all other rock-forming minerals, there is no correlation between the host phase and the age or chemistry (including Zr) of the included rutile within any rock. A plurality of rutile analytical spots sampled various microinclusions of other phases (particularly zircon); all data in Figure 8 and Table S5 have been screened for inclusions, though there are still many inclusion-free spots that contain significant common Pb. Rutile U-Pb dates for the foliated mafic eclogites are imprecise due to low U and also potentially inaccurate due to Pb\* loss, with horizontal arrays drawn away from the discordia lines defined by the oldest spots in each sample. As such, the mafic eclogite discordia dates in Figures 8a and 8b (79.1  $\pm$  5.1 Ma, MSWD = 0.43; 75.9  $\pm$  3.8 Ma, MSWD = 0.79) are calculated from a small subset of the oldest spots (n = 5 for each sample); therefore, the calculated dates only provide minimum constraints on the timing of rutile growth or U-Pb system closure. The more U-rich rutile grains in the quartz-bearing foliated eclogite also produced few inclusion-free spots and thus yield a poorly resolved rutile U-Pb date (80  $\pm$  12, n = 5, MSWD = 2.6) (Figure 8c). In contrast, the granoblastic eclogite and metafelsite data provide tighter U-Pb age constraints with slightly younger dates for the eclogites (76.9  $\pm$  1.1 Ma, n = 23, MSWD = 0.85; 75.9  $\pm$  2.1 Ma; n = 10, MSWD = 1.3) than the metafelsite  $(78.7 \pm 0.9 \text{ Ma}; n = 28, \text{MSWD} = 0.84)$  (Figures 8d–8f). Each of these latter dates forms a statistical single population (Wendt & Carl, 1991).

As noted for U (Figures 8a–8f), the clearest first-order variation in rutile trace elements is characterized by the gradation from mafic to felsic bulk compositions. However, the mean Zr concentration is uniform across the entire population (Figure 8g), despite the fact that two of the eclogites lack extant quartz, which should nominally increase the equilibrium Zr concentration in rutile relative to a quartz-bearing rock at the same P-T-a(ZrSiO<sub>4</sub>) (Ferry & Watson, 2007). Instead, these observations suggest that quartz was saturated in all rocks during rutile growth. Using the Tomkins et al. (2007) calibration of the Zr-in-rutile thermobarometer for the  $\alpha$ -quartz field,  $P = 20 \pm 2$  kbar (suggested by eclogite phase equilibria Warren & Waters, 2006), and a(SiO<sub>2</sub>) = a(ZrSiO<sub>4</sub>) = 1, the data yield a mean Zr-in-rt  $T = 520 \pm 18$ °C. Using slightly higher metamorphic pressures ( $P = 25 \pm 2$  kbar) calculated from pseudosections of the metafelsite (Massonne et al., 2013), the cal-

Figure 7. Zircon CL, U-Pb, and trace-element results (LASS) for foliated quartz-bearing eclogite CWO21 (a–d) and metafelsite 131219J02 (e–g). (a) CL images of CWO21 zircons displaying "soccer-ball"-like sector and fir-tree zoning. (b) Tera-Wasserburg concordia diagram of CWO21 zircon data, showing a significant spread along concordia that does not form a single population; the location of each spot along the concordia curve is independent of any trace element data. A weighted-mean date from the same sample (c) yields the same date within uncertainty, but with tighter error bounds; we therefore adopt the lower-intercept date and its uncertainty in (b) as a more conservative average date. (d) Chondrite-normalized (McDonough & Sun, 1995) REE patterns for CWO21 zircons, displaying relatively homogeneous patterns with a Ce anomaly but lacking a Eu anomaly. (e) CL images of 131219J02 zircon, displaying faint CL-dark rims on oscillatory, concentric, and/or sector-zoned CL-bright cores. (f) Tera-Wasserburg concordia diagram of 131219J02 zircon data, showing clearly delineated younger rims (depth profiling data) and several clusters of older zircon cores (spot data). (g) Chondrite-normalized REE patterns for 131219J02 zircons, with trace-element poor, young rims (blue) and trace-element rich, older cores (with colors corresponding to different U-Pb dates). All data used to construct these plots are contained in Tables S3 and S4.

GARBER ET AL. 13 of 26



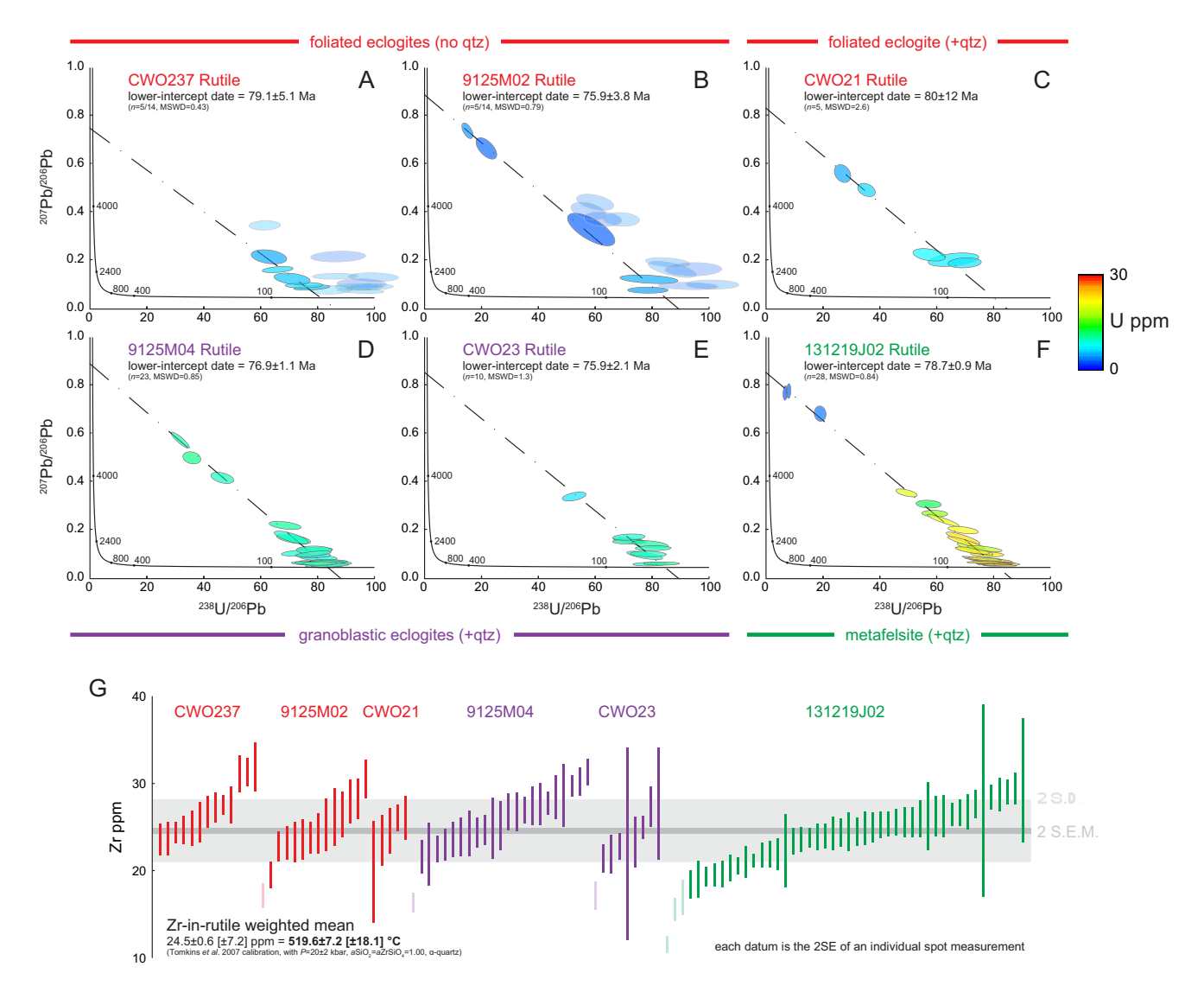


**Figure 8.** Rutile U-Pb and trace-element results (LASS) arranged from the most mafic (a) to the most felsic (f) lithologies at As Sifah. Zr-in-rutile thermobarometry data (g) are shown for the same samples. Data in panels (a) and (b) that were excluded from the isochron regression are shown with increased transparency. All data used to construct these plots are contained in Table S5.

culated temperatures are  $\sim 20^{\circ}$ C higher (540  $\pm$  18°C); using slightly lower metamorphic pressures calculated from mafic eclogite phase equilibria (maximum P=16 kbar) (El-Shazly, 2001) yields temperatures  $\sim 15^{\circ}$ C lower (506  $\pm$  16°C).

# 6. Discussion

# 6.1. Radiometric Dates and the Timing of Metamorphism Recorded by As Sifah Eclogites

The data presented in this study support the interpretation that peak to early retrograde metamorphism occurred at  $\sim$ 81–77 Ma, variably recorded by different rocks, different metamorphic minerals, and different isotopic systems. Each result is summarized and interpreted below and displayed graphically in Figure 9.

# **6.1.1.** Garnet

Statistically significant, five- to seven-point garnet-WR(-glaucophane) Sm-Nd isochrons define a range of garnet growth ages from  $80.9 \pm 1.3$  Ma (metafelsite 131219J02) to  $79.0 \pm 3.2$  Ma (granoblastic eclogite

GARBER ET AL. 14 of 26

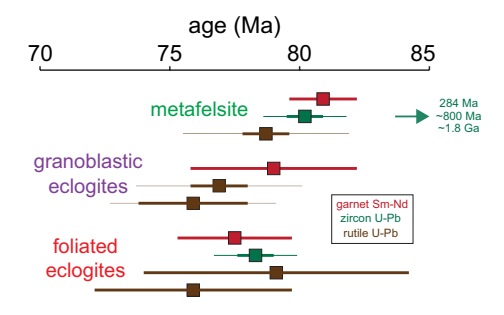


Figure 9. Summary of age results for the samples in this study (with one imprecise rutile U-Pb date omitted from the foliated eclogites). Internal  $2\sigma$  uncertainties are shown in a thicker line, with systematic uncertainties shown for zircon U-Pb (2%) and rutile U-Pb (4%) in thinner lines; no additional uncertainty is added to the garnet Sm-Nd dates because the age calculation includes external errors, and mafic rutile U-Pb dates have internal uncertainties that exceed external ones. Each data set shows a progression from older dates in the metafelsite to younger in the eclogites, while the eclogites show a decrease in rutile U-Pb age precision due to lower U and more significant Pb\* loss.

9125M04) to 77.5  $\pm$  2.2 Ma (foliated eclogite CWO237) (Figure 6a). These bulk-separate ages can be broadly interpreted as an "average" over the duration of garnet growth, but in detail, the calculated ages depend on the distribution of Sm in garnet, the garnet crystal size distributions, parent and/or daughter diffusion, and the effects of inherited phases. The latter two factors are likely insignificant here: relatively cool peak metamorphic temperatures (~500–600°C) (El-Shazly, 2001; Massonne et al., 2013; Searle et al., 1994; Warren and Waters, 2006) preclude a significant volume diffusion of either Sm or Nd over the timescales of As Sifah metamorphism (e.g., Bloch & Ganguly, 2015), and both tabletop and bombed whole-rock aliquots plot nearly in the same place for all samples, suggesting the whole-rock Nd isotope equilibrium and the exclusion of any inherited Nd isotopic signature. Calculation of crystal size distributions and their relationship with the timing of garnet growth are beyond the scope of this study and are likely to be complicated by early nucleation and crystal growth processes that are now overprinted (Carlson, 2011); we therefore ignore these effects.

The LA-ICPMS data show that Sm distributions are biased toward garnet rims (Figures 4 and 5), such that the Sm-Nd dates are dominated by the outer 20–40 radial % of the bulk garnet population in each sample. Based on

rock textures, garnet major-element data, and conventional thermobarometry, these garnet rims have been interpreted to record the timing of peak to early retrograde metamorphism in the As Sifah eclogites (Warren and Waters, 2006; Massonne et al., 2013). This interpretation is consistent with our textural observations, including (a) cpx-rt inclusions at garnet rims in the eclogites and (b) the growth of a late, hydrous assemblage (phg-gl-ep) associated with partial garnet rim resorption. The garnet Sm distributions are not identical in all samples, but their variation does not appear to correlate with date; for example, the granoblastic eclogite with more rim-biased Sm distributions (9125M04) yielded an older Sm-Nd date than the foliated eclogite with more core-biased Sm abundances (CWO237) (Figures 5 and 6). Instead, the progression in Sm-Nd date correlates solely with lithology, as do  $\varepsilon_{Nd}$  and the sample-averaged garnet  $^{147}$ Sm/ $^{144}$ Nd (Figure 6a). Because these different lithologies appear to be a part of the same stratigraphic horizon that is traceable throughout the entire As Sifah and Hulw Windows (e.g., Miller et al., 1999) and were thus juxtaposed well prior to metamorphism, these distinctions in garnet ages between more felsic and more mafic samples could arise from differences in the timing of the garnet-forming reaction in different bulk compositions, because garnet is expected to grow at lower grade P-T conditions in the metafelsite (Massonne et al., 2013) than the mafic eclogites (Warren and Waters, 2006). These differences could also arise from kinetic factors, such as heterogeneous reaction overstepping among lithologies (Pattison & Tinkham, 2009). Considering these factors, the Sm-Nd dates represent rim-biased average garnet growth ages for each lithology and suggest that peak conditions—and the volumetric bulk of garnet growth—occurred between ~81 and 77 Ma.

# **6.1.2.** Zircon

The zircon LASS data (depth profiles and spots) further bracket the timing of garnet growth with the ages and trace elements supporting the Sm-Nd garnet-WR isochron ages. Zircon grains from quartz-bearing foliated eclogite CWO21 yield an array of dates from  $\sim$ 85 to 75 Ma with an "average" lower intercept date of 78.3  $\pm$  0.7 Ma (Figure 7b). This LA-ICPMS date is within the uncertainty of ID-TIMS U-Pb concordia dates on the same sample (79.06  $\pm$  0.32 Ma) (Warren et al., 2003) as well as garnet Sm-Nd dates from both the foliated (77.5  $\pm$  2.2 Ma) and granoblastic eclogites (79.0  $\pm$  3.2 Ma). The zircon morphologies and CL zoning (Figure 7a) are consistent with precipitation from a metamorphic fluid (Rubatto, 2017) as previously suggested (Warren et al., 2005). This is further consistent with the abundance of hydrous phases in the mafic eclogites. Trace elements from these zircons are nearly congruent across the entire population: significant HREE depletions in all grains (Figure 7d) implicate the influence of garnet prior to or during zircon growth, and the absence of an Eu anomaly suggests the consumption of plagioclase by that time (Rubatto & Hermann, 2007; Taylor et al., 2017). Textural observations also clarify that zircon is associated with the peak metamorphic assemblage in each rock, with zircon grains included

GARBER ET AL. 15 of 26



in garnet and clinopyroxene and in turn containing rutile inclusions (Warren et al., 2003). The data therefore suggest that the foliated eclogite zircon U-Pb dates—both LA-ICPMS and TIMS—represent peak metamorphic crystallization ages coincident with garnet growth.

However, we are skeptical that the  $\sim 10$  Myr apparent range in LA-ICPMS dates is geologically significant. Rutile U-Pb systematics from the mafic eclogites are also disturbed (Figures 8a–8c; see below), and it is difficult to conceive of continuous, protracted precipitation of individual sector-zoned zircons from a metamorphic fluid over  $\sim 10$  My (as the entire range in date is observed within single crystals). Mafic eclogite zircons with similar morphologies and sector zoning—and in similar rocks and tectonic settings—generally give punctuated dates (<1 Myr) representing discrete fluid pulses (e.g., Rubatto & Hermann, 2003; Rubatto & Angiboust, 2015; Garber, Smye, et al., 2020). Furthermore, the single-population zircon U-Pb TIMS date from Warren et al. (2003) on the same zircons (that is within uncertainty of our average LA-ICPMS date) further suggests that the zircons do form a single age population. As such we interpret only the average LA-ICPMS date (78.3  $\pm$  0.7 Ma) and not the apparent range exhibited by this sample.

We note that the calculated CWO21 Ti-in-zircon temperatures (~610–620°C) are also consistent with growth during peak metamorphic conditions, but exceed all other thermometry on the As Sifah eclogites, including the Zr-in-rutile temperatures from the same rocks in this study. The expected zircon Ti concentrations for the peak temperatures calculated from thermodynamic modeling (~550°C) are extremely low (<1 ppm); the measured Ti contents in these grains are slightly higher than this (~2 ppm), and we propose that they may be affected by rutile micro-inclusions that are difficult to filter from the data, as these are observed in BSE images of these zircon grains (Warren et al., 2003). We therefore interpret Ti-in-zircon temperatures from this sample semiquantitatively, that is, only to support the growth of zircon at the relatively cool (~500–600°C) peak metamorphic temperatures determined by other methods.

Concordant U-Pb analyses from sector- to oscillatory-zoned zircon cores in the end-member metafelsite (131219J02; Figure 7e) yield three distinct sets of dates, with rare ~1.8 Ga and ~800 Ma grains and a dominant  $283.8 \pm 0.7$  Ma population. The trace elements associated with each of these populations suggest igneous rather than metamorphic zircon crystallization, particularly the significant negative Eu anomalies, elevated Th/U, and the absence of HREE depletions. The ~1.8 Ga date is common in detrital and xenocrystic igneous zircon populations throughout the Arabian plate (Stern & Johnson, 2010). The ~800 Ma population matches the timing of magmatic and metamorphic activity associated with the Mirbat Granulite Complex in southwestern Oman (Mercolli et al., 2006; Bowring et al., 2007), which is the largest exposure of Proterozoic deep crust in eastern Arabia. These dates have been interpreted to represent the timing of continental lithosphere stabilization in E. Arabia, as there are few regional deep-crustal rocks with dates younger than 750 Ma (Stern & Johnson, 2010 and references therein). The youngest zircon core population (283.8  $\pm$  0.7 Ma; n = 83) is by far the most dominant; it is consistent with the interpretation of a tuffaceous protolith (Le Metour et al., 1986) and suggests that the older zircon populations represent magmatic xenocrysts. This date is significantly younger than the SHRIMP U-Pb zircon crystallization date of 298 ± 3 Ma from the same metatuff horizon at As Sifah beach (Gray, Gregory, Armstrong, et al., 2005). We cannot determine if these interstudy age differences are geologic—for example, if there were multiple discrete tuffs emplaced over ~15 My—or if they reflect analytical biases between LA-ICPMS and SHRIMP data that were collected ~15 years apart and referenced to difference zircon U-Pb standards. However, though we are not aware of other similarly aged volcanics in NE Oman, zircon dates from both this study and Gray, Gregory, Armstrong, et al. (2005) bracket other records of deglaciation and rifting associated with the breakup of Pangaea and the opening of the Neotethys during the Permian (Angiolini et al., 2003). For example, using brachiopod biostratigraphy of the Al-Khlata and Saiwan Formations (Haushi Group) in interior Oman, Angiolini et al. (2003) determined a late Sakmarian age for the initiation of rifting (~295-290 Ma), which is younger than the Gray, Gregory, Armstrong, et al. (2005) dates but older than our new ages. Therefore, regardless of the distinctions in measured protolith dates, all of them demonstrate that the metafelsite marks a key stratigraphic horizon: it delineates the same pre-Permian unconformity exposed throughout the Saih Hatat and the broader Arabian rock record (e.g., Searle et al., 2004).

Young zircon rims from the metafelsite ( $80.2 \pm 0.7$  Ma) form a single age- and trace-element population with low Th/U and lower REE concentrations relative to the igneous cores—consistent with metamorphic (re)crystal-lization—but lack HREE depletions expected from the influence of garnet growth. This is unexpected because

GARBER ET AL. 16 of 26



the Sm-Nd garnet growth age  $(80.9 \pm 1.3 \text{ Ma})$  from the same sample overlaps the U-Pb date within uncertainty. It is possible that zircon grew immediately before garnet, in which case the zircon date would bracket the start of garnet growth. Alternatively, the amount of garnet may not have been sufficient to deplete the whole-rock HREE budget by the time zircon crystallized, or the zircon may have grown during an initial phase of exhumation-related garnet breakdown immediately postdating garnet growth. However, it is as likely that the REE did not entirely achieve chemical equilibrium during zircon (re)crystallization, which has frequently been observed in other high-P altered zircons that retain a trace-element "memory" of their precursors, even in the presence of garnet (Chen et al., 2010; Štípská et al., 2016; Garber, Smye, et al., 2020). We therefore suggest that—such as those in the eclogites—the metafelsite zircons record (re)crystallization during the growth of the peak metamorphic assemblage (garnet-phengite-quartz), which slightly preceded garnet and zircon (re)crystallization in the eclogites. The absence of any ages between ~284 and 80 Ma suggests that there were no zircon-forming metamorphic events during that interval.

# **6.1.3.** Rutile

The calculated rutile U-Pb isochron dates span  $\sim 80-76$  Ma, broadly matching the Sm-Nd garnet and U-Pb zircon dates. In detail, however, the most foliated eclogites yield imprecise dates with clear evidence for radiogenic Pb loss (Figures 8a-8c), while the granoblastic eclogites and metafelsite rutile dates are more precise (Figures 8d-8f) and show a similar age pattern to the garnet and zircon data, with an older metafelsite age (78.7  $\pm$  0.9 Ma) and younger eclogite ages (76.9  $\pm$  1.1 Ma; 75.9  $\pm$  2.1 Ma) that each forms a statistical single population. There is also a progression in rutile trace-element composition across bulk compositions, particularly notable in the increasing U content from mafic to felsic rutile.

Because Pb loss can be significant in rutile at eclogite-facies conditions (Cherniak, 2000; Smye et al., 2018), we modeled Pb diffusion to assess whether the rutile U-Pb dates are cooling or crystallization ages. Zircon fission-track dates from the As Sifah and Hulw Windows yield extremely reproducible, 66-70 Ma dates, suggesting that all samples experienced ≥30°C/My cooling from eclogite-facies conditions (Saddiqi et al., 2006), which we adopt as a minimum cooling rate. Additionally, though the analyzed rutile grains are of variable sizes, all have at least one radial dimension <25 μm, which we adopt as the maximum diffusion radius. Using the Dodson (1973) formula for diffusive closure temperatures, a spherical grain geometry, diffusion parameters for Pb in rutile from Cherniak (2000),  $dT/dt = 30^{\circ}C/My$ , and  $r = 10-25 \mu m$ , the effective Pb closure temperature for the As Sifah rutiles is ~560–600°C; faster cooling rates would yield higher closure temperatures. This is higher than the Zr-in-rutile temperature determined for the same grains (520 ± 18°C; Figure 8g) as well as temperatures determined by conventional thermobarometry (~500-560°C) (Massonne et al., 2013; Warren and Waters, 2006), nominally suggesting minimal Pb loss during cooling. This is supported by the absence of systematic differences in rutile grain size between the different lithologies, and rutile spots shifted horizontally away from concordia in the foliated eclogites (Figures 8a-8c) do not systematically occur in smaller grains. Critically, though there are lithology-based rutile U-Pb age differences, the entire mafic-to-felsic suite appears to have been juxtaposed since protolith emplacement: the same unit is traceable throughout the entire Hulw-As Sifah Window section (Figure 1), and there are relict volcanic textures in lower grade exposures (Gray, Gregory, Armstrong, et al., 2005; Miller et al., 2002; Warren & Miller, 2007). Therefore, even if the eclogites and metafelsites transformed to peak metamorphic assemblages at slightly different times—as suggested by the Sm-Nd garnet and U-Pb zircon dates—it is difficult to imagine that they would also have cooled through rutile Pb closure from peak T at different times if they were continuously juxtaposed, i.e., to yield the resolvable differences in rutile U-Pb date.

These observations suggest that the rutile U-Pb isochron dates are primarily crystallization ages with minor Pb\* loss, most demonstrably in the mafic rutile grains. The rutile ages postdate Sm-Nd and U-Pb dates from the same rocks (Figure 9), but this may be explained partly by systematic offsets, with far higher external uncertainties on rutile dates relative to garnet or zircon dates. The preferential mafic-rutile Pb\* loss is difficult to explain with our data alone; it could imply shorter effective diffusion radii, which—if not related to macroscale grain size—could arise from exsolved lamellae of other phases (e.g., ilmenite) or deformation-related features (e.g., dislocations). We note that mafic eclogites from As Sifah show several age disturbances in multiple isotopic systems, including (a) extraneous Ar in phengite, particularly in mafic eclogites (e.g., Warren et al., 2011), and (b) dispersed zircon LA-ICPMS U-Pb data along concordia (Figure 7b). The Ar isotopic signatures have been shown to relate to dif-

GARBER ET AL. 17 of 26



ferences in mafic vs. pelitic devolatilization behaviors during subduction (Smye et al., 2013), and it is possible that the processes leading to extraneous Ar in mafic rocks also affected the Pb\* systematics in rutile and zircon. In this case, the rutile U-Pb isotopic dates may reflect the timing of fluid alteration that persisted longer or more significantly in the eclogites than the metapelite, which is supported by the ubiquitous occurrence of texturally late epidote in the foliated mafic eclogites (Table 1).

# 6.1.4. Age Summary

The three petrochronological data sets presented here—isotopic dates (Sm-Nd, U-Pb) and trace elements from garnet, zircon, and rutile—suggest the emplacement of the metafelsite protolith at  $283.8 \pm 1.7$  Ma, and the growth of peak garnet-bearing assemblages in all As Sifah beach rocks from ~81 to 77 Ma. There are minor lithologically controlled age variations, with the end-member metafelsite recording the earliest metamorphism in each data set (Sm-Nd garnet:  $80.9 \pm 1.3$  Ma; U-Pb zircon:  $80.2 \pm 0.7[\pm 1.6]$  Ma; and U-Pb rutile:  $78.7 \pm 0.9[\pm 2.4]$  Ma) and the foliated eclogites recording the most recent (Sm-Nd garnet:  $77.5 \pm 2.2$  Ma; U-Pb zircon:  $78.3 \pm 0.7[\pm 1.6]$  Ma; U-Pb rutile: imprecise and affected by Pb loss). Because the mafic and felsic end-members were almost certainly in contact prior to metamorphism, these data support thermodynamic (different garnet-forming reactions) or kinetic heterogeneities (reaction overstepping). Regardless of their origin, the consistent age differences among all analyzed phases suggest that each rock transformed to peak metamorphic assemblages within a narrow time frame.

## 6.2. The Case of a Single Metamorphic Event in the Saih Hatat

Several authors have proposed the existence of two metamorphic events in the Saih Hatat, one at ~120–110 Ma and the other at ~80 Ma (Figure 2). This earlier metamorphic event has also been hypothesized to result from continent-ward (SW-directed) subduction (Gray, Miller, et al., 2004; Goscombe et al., 2020), which would have significant implications for the history of the Samail Ophiolite and much of the recent geological history of Oman. Critically, this tectonic hypothesis is based on which of the available geochronology of the As Sifah Window is considered robust and representative, including previously measured Sm-Nd, Ar/Ar, U-Pb, and Rb-Sr dates. Below, we highlight what we consider the most significant geochronological weaknesses in the case for an ~110 Ma metamorphic event, based partly but not exclusively on our data.

- 1. The main line of evidence for the ~110 Ma metamorphic event is two Sm-Nd garnet-WR-leachate dates from foliated and granoblastic eclogites at  $110 \pm 9$  and  $109 \pm 13$  Ma, respectively (Gray, Hand, et al., 2004). These data are shown with our new results in Figure 6. Having sampled a representative textural and lithologic range, our garnet isotopic data plot at significantly higher average  $^{147}$ Sm/ $^{144}$ Nd, yield more precise and statistically significant dates, and have internally consistent  $\varepsilon_{Nd}$  that varies with lithology. In short, for non-geological reasons alone, we contend that the Gray, Hand, et al. (2004) ~110 Ma Sm-Nd dates are not geologically meaningful. We also note two analytical issues with the existing Gray et al. Sm-Nd dates:
  - (a) The Gray et al. data used to calculate the ~110 Ma dates scatter between the isotopic end-members defined by our samples (Figure 6b), such that the garnet and whole-rock aliquots could have sampled different reservoirs that were not in isotopic equilibrium during metamorphism. This can be assessed by comparing <sup>143</sup>Nd/<sup>144</sup>Nd against 1/[Nd] (Figure S3 in Supporting Information S1), which shows that the garnet and leachate aliquots used to define the Gray et al. dates form clear mixing lines with the whole-rock aliquot. We note that our data form apparent mixing lines on this type of plot, but this is due to the better separation of garnet and whole-rock aliquots relative to Gray et al., creating two distinct clusters of data that roughly define a line. However, our data are not colinear in detail, and the three parallel isochrons with clear initial isotopic separation between samples (Figure 6a) preclude mixing to explain our data.
  - (b) Multiple garnet aliquots from single samples in Gray et al each plot in exactly the same place (Figure 6b). This is highly unlikely because it would require that each 100–300 mg garnet aliquot had exactly the same proportion of garnet core and rim material, given that cores and rims have different proportions and concentrations of Sm and Nd (e.g., Figures 4 and 5). In contrast, our garnet data scatter along the <sup>147</sup>Sm/<sup>144</sup>Nd axis, consistent with the sampling of variable core and rim proportions in our garnet separate (Figure 6a).

GARBER ET AL. 18 of 26



- 2. The new zircon trace-element data demonstrate the influence of garnet during precipitation from a metamorphic fluid in the foliated eclogite samples (Figures 7b and 7d), while the metafelsite zircon rims nominally escaped HREE resetting (Figures 7f and 7g). However, both are within the uncertainty of Sm-Nd garnet dates for the same samples (Figure 8) and the trace-element observations are similar to those in other high-*P* zircons (Chen et al., 2010), suggesting that the zircons grew synchronously with garnets—not during exhumation ~30 My later as suggested by Gray, Hand, et al. (2004) and Gray, Miller, et al. (2004).
- 3. Rutile is unambiguously part of the peak, high-*P* assemblage in all the As Sifah rocks (see sample descriptions and Figure 3). Because the rutile closure T to Pb diffusion in these rutile grains is similar to the peak metamorphic temperature (~550–600°C), any metamorphism prior to the ~81–77 Ma event should have been preserved, that is, it would not have been totally reset, given the subsequent *T-t* history of the As Sifah eclogites. The absence of age inheritance in rutile thus supports only a single metamorphic event.
- 4. The other data set that has been used to support the ~110 Ma event is Ar/Ar dating (Miller et al., 1998; Miller et al., 1999; Gray, Miller, et al., 2004), but there are well-known issues with Ar/Ar dating in high-*P* rocks—and there have been detailed studies of grain-scale extraneous Ar in the As Sifah eclogites showing that the older ages are inaccurate and insignificant (Warren et al., 2011). These issues are particularly problematic in more mafic lithologies due to closed-system fluid behavior, as mafic rocks are thought to preferentially retain fluids and trap more excess Ar during high-pressure metamorphism relative to felsic or pelitic protoliths (Smye et al., 2013). This lithological effect may also partly explain the zircon and rutile U-Pb results (see above). Importantly, the Ar/Ar dates from the structurally highest, lowest pressure nappes contain exclusively ∼80 Ma phengite dates (e.g., El-Shazly & Lanphere, 1992), which are consistent with the increasing effect of excess Ar with increasing metamorphic pressure (e.g., Sherlock et al., 1999; El-Shazly et al., 2001). Together, these observations suggest that the Ar/Ar dates from As Sifah eclogites do not date continental subduction in the Saih Hatat.

In summary, all demonstrably robust geochronological and geochemical data (including Sm-Nd, U-Pb, and Rb-Sr results: El-Shazly et al., 2001; Warren et al., 2003; Warren et al., 2005, and this study) support the subduction of the Arabian continental margin to eclogite-facies conditions at ~81–77 Ma, after the crystallization of the Samail Ophiolite at ~96.2–95.0 Ma (Rioux et al., 2012; Rioux et al., 2013; Rioux, Garber, et al., 2021) that overlies the Saih Hatat collisional orogen. This conclusion is supported by other data sets not addressed here, including multiple structural and stratigraphic arguments that preclude such significant tectonism at 120–110 Ma (see Searle et al., 2004, 2005). Still, we emphasize that this hypothesis is untenable from a geochronological perspective alone, and that there is simply no evidence for early continent-ward subduction in Oman.

# 6.3. Rates of Prograde Subduction and Retrograde Exhumation

The deep (U)HP subduction and exhumation of continental material—including "continental crust" in a strict sense, and continental margin rocks more broadly—has been shown to occur at a range of rates that typically correlate with the size of the subducted body and orogenic stage, such that smaller fragments subducted earlier in an orogenic event typically do so faster (e.g., Dora Maira: Rubatto & Hermann, 2001; Gauthiez-Putallaz et al., 2016) than larger, later (U)HP bodies (e.g., Western Gneiss Region, Norway: Kylander-Clark et al., 2008; Kylander-Clark et al., 2009) (see also Kylander-Clark et al., 2012). With our new data emphasizing the late absolute timing of continental subduction and exhumation of the As Sifah eclogites beneath the Samail Ophiolite, we conclude by considering the possible rates at which this process occurred. A summary of available tectonic and geochronological constraints on the subduction of the As Sifah rocks is shown in Figure 10.

The timing at which prograde continental subduction initiated can only be broadly constrained. It is unlikely that the As Sifah-Hulw protoliths were subducted prior to the formation of the metamorphic sole in the overlying ophiolite, as these rocks record proto-subduction geotherms far hotter than those experienced by the As Sifah eclogites (Ambrose et al., 2021; Cowan et al., 2014; Soret et al., 2017). For example, a metapelite in the sole of the Wadi Tayin massif—which structurally overlies the Saih Hatat—experienced metamorphic conditions of

GARBER ET AL. 19 of 26



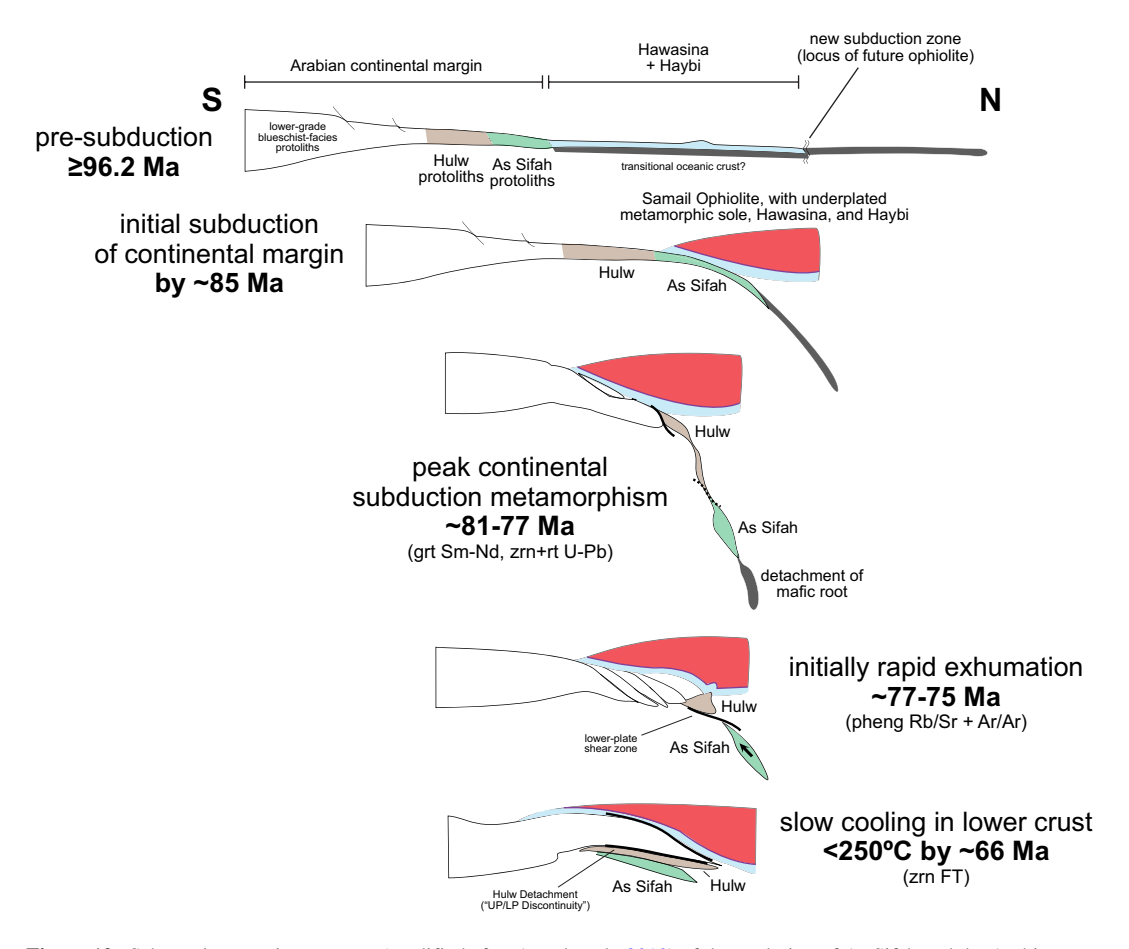


**Figure 10.** Schematic tectonic summary (modified after Agard et al., 2010) of the evolution of As Sifah and the Arabian margin prior to, during, and after continental subduction. Constraints on each evolutionary stage are discussed further in the text.

 $7.5 \pm 1.2$  kbar,  $665 \pm 32^{\circ}$ C as late as  $\sim 93.0 \pm 0.5$  Ma (Garber, Rioux, et al., 2020). Additionally, there are texturally crosscutting metasediment melts that intruded the Samail Ophiolite as late as  $\sim 95.0$  Ma (Haase et al., 2015; Rollinson, 2009; Rollinson, 2015; Rioux, Benoit, et al., 2021; Rioux, Garber, et al., 2021; Spencer et al., 2017). As the ophiolite broadly represents the structurally highest thrust sheet under which the As Sifah eclogites subducted (Agard et al., 2010; Searle et al., 2004), these data represent firm bounds on the initiation of continental subduction and further coincide with the stratigraphic record for downwarping of the continental margin in response to the approaching ophiolite by the Turonian ( $\sim 94-90$  Ma: Robertson, 1987). Considering initial subduction of the margin starting at  $\sim 95.0-93.0$  Ma, with material reaching peak conditions ( $\sim 2.0-2.5$  GPa; 60-80 km assuming lithostatic pressures) by  $\sim 81-77$  Ma, and assuming a relatively shallow subduction angle  $(20-30^{\circ}$ ; see e.g., Hu & Gurnis, 2020) yields vertical sinking rates of  $5 \pm 2$  mm/yr and convergence rates of  $\sim 10-20$  mm/yr.

These rates are obvious minima because continental subduction may have started significantly after ~95–93 Ma, i.e., much closer to the timing of peak metamorphism by ~81 Ma. Indeed, the above-calculated convergence rates are less than total Arabia-Eurasia convergence at ~85–80 Ma (~30–50 mm/yr: Agard et al., 2007), although some of this convergence was probably accommodated along the Makran subduction zone further to the north. Combining the same contraints as above with the fastest possible convergence rate (50 mm/yr) would require that prograde continental subduction commenced after ~85–84 Ma, which represents a maximum timing constraint. Though broad, this range of possible As Sifah sinking rates (~5–30 mm/yr) exceeds those from giant *UHP* terranes such as the Western Gneiss Region (2–4 mm/yr: Kylander-Clark et al., 2009), but they match several *HP-UHP* Alpine exposures (>5 mm/yr: Lago di Cignana, Sesia-Lanzo, Dora Maira)

GARBER ET AL. 20 of 26



(Gauthiez-Putallaz et al., 2016; Lapen et al., 2003; Rubatto et al., 2011). Notably, the observed mineral assemblages and calculated P-T conditions for these small Alpine HP-UHP bodies are similar to those calculated for As Sifah, for example, the Zermatt-Saas (Angiboust et al., 2009) and Monviso ophiolites (Angiboust et al., 2012), as well as Corsican lawsonite eclogites and garnet blueschists (Vitale-Brovarone et al., 2011). This broadly suggests that the prograde subduction of As Sifah occurred similarly to other small HP-UHP bodies, with continental materials dragged to mantle depths by a denser mafic slab that later detached (e.g., Duretz et al., 2016).

Exhumation rates are likewise difficult to calculate accurately because there are few barometric constraints on the retrograde eclogite path. If taken as thermochronometers, the coincidence between existing phengite-whole rock Rb-Sr (78 ± 2 Ma: El-Shazly et al., 2001) and minimum Ar/Ar plateau dates (~77-79 Ma: El-Shazly & Lanphere, 1992; Miller et al., 1999) represents extremely fast cooling below their respective closure temperatures (~500°C and ~400–350°C, respectively). Combining these dates with the evidence for crystallization of peak assemblages at ~500-600°C from ~81 to 77 Ma (this study) suggests initial cooling rates up to  $\sim 100^{\circ}$  C/My, requiring an initial but unquantifiable phase of rapid exhumation from mantle depths. At the same time, it is also possible that the phengite Rb-Sr and Ar/Ar record the last timing of fluid-rock interaction with the extant assemblage rather than a cooling age. For example, Glodny et al., (2008) showed that ~900-950 Ma granulite-facies rocks only experienced ~400 Ma Rb-Sr isotopic resetting along fluid alteration zones, even as metamorphism exceeded >650°C for several Myr; similar cases exist for the Ar/Ar system (e.g., Villa, 2010). In this case, the coincidence in the youngest Sm-Nd, U-Pb, Rb-Sr, and Ar/Ar dates and the modest peak metamorphic temperatures (~500-600°C) might suggest synchronous (re)crystallization of these phases in the presence of a fluid from ~81 to 77 Ma, with exhumation only occurring after ~77 Ma. However, even if none of the dates are cooling ages, there is circumstantial evidence to suggest an initially rapid phase of exhumation—particularly that the As Sifah rocks are bounded by abundant carbonates and calcschists that maintain buoyancy and can accommodate significant strain even after a complete transformation to HP parageneses.

Other more demonstrably thermochronometric dates are significantly younger: zircon fission-track dates for the As Sifah and Hulw Windows yield a consistent, reproducible  $68 \pm 6$  Ma ( $2\sigma$ ) cooling age though  $\sim 260^{\circ}$ C (Saddigi et al., 2006); under any reasonable post-orogenic geotherm, these temperatures would have been attained at <5 kbar (<15 km), firmly placing both "lower-plate" units adjacent to each other in the middle crust by that time. Apatite fission-track dates further suggest cooling below  $\sim 60^{\circ}$ C by  $\sim 53$  Ma but are as young as  $\sim 40$  Ma (Poupeau et al., 1998). If the youngest Ar/Ar dates reflect cooling below ~350°C, these data suggest a long crustal residence time before the exposure of the As Sifah and Hulw Windows at the surface (~40 My), with an attendant, sharp decrease in cooling rate ( $<10^{\circ}$ C/My) after initially rapid exhumation from peak P conditions (see also El-Shazly et al., 2001). This slow upward transit through the crust contrasts with the global record of fast exhumation recorded in small UHP bodies (e.g., Kylander-Clark et al., 2012) and likely relates to key tectonic differences between As Sifah and other (U)HP exposures. For example, whereas the upper plate of many (U)HPorogens appears to undergo significant extension during exhumation (Johnston et al., 2007; Young et al., 2011; Young, 2017), the Samail Ophiolite and its cover experienced relatively little extension during emplacement (Fournier et al., 2006). To this point, the "extensional" S-C fabrics present throughout the As Sifah eclogites and enclosing calc-schists are related to exhumation of footwall rocks toward the SW rather than any significant extension of the overlying crust (Searle et al., 2004; Searle, 2007). At the same time, the subduction of the As Sifah rocks coincided with a significant (20-40 mm/yr) decrease in the Arabia-Eurasia convergence rate (Agard et al., 2007), such that there were fewer far-field stresses driving extension of the upper plate as the As Sifah rocks exhumed.

## 7. Conclusions

1. Sm-Nd, U-Pb, and trace-element analyses of garnet, zircon, and rutile from As Sifah eclogites (NE Oman) record ~81–77 Ma peak to early retrograde metamorphism. There are consistent lithology-based age, mineralogical, and textural differences that suggest a bulk-compositional or kinetic control on the timing of

GARBER ET AL. 21 of 26



- the peak assemblage in each lithology, but all the data suggest relatively punctuated transformation in each rock.
- 2. Protolith zircon dates for the felsic metatuff (283.3 ± 0.7 Ma) suggest that the As Sifah eclogites mark the pre-Permian unconformity exposed throughout NE Oman, consistent with its derivation from a more distal exposure of the same rocks exposed elsewhere in the Saih Hatat.
- 3. There is no evidence for an ~110 Ma metamorphic episode in the As Sifah Unit; our new Sm-Nd dates show internally consistent features and cover the range of metamorphic histories preserved at As Sifah, indicating that previously published Sm-Nd dates are inaccurate. All demonstrably robust geochronology is consistent with only a single metamorphic event, in which the Arabian continental margin subducted toward the NE beneath the already emplaced Samail Ophiolite by ~81–77 Ma.
- 4. A comparison between As Sifah and other small (U)HP continental subduction orogens suggests that As Sifah underwent a relatively similar prograde tectonic evolution to similar small (U)HP bodies (e.g., W. Alps), with subsequently rapid exhumation to the lower crust, followed by significantly slower exhumation to the upper crust. This long crustal residence time likely reflects tectonic conditions unique to As Sifah, including a decrease in convergence rate during subduction of the Arabian margin to mantle depths, and the absence of significant upper crustal extension as As Sifah exhumed.

# **Conflict of Interest**

The authors declare no conflicts of interest relevant to this study

# **Data Availability Statement**

All data supporting the conclusions in this paper (Tables 1–2, Table S1–S5) are freely available online at doi: 10.17605/OSF.IO/CZG3P.

# Acknowledgments References

This paper is dedicated to the memory of

Dr. Adolphe Nicolas, who-in collabo-

ration with Dr. Françoise Boudier-was

instrumental in introducing the first and

second authors to the geology of Oman

commentary as this manuscript was being

assembled. We thank the Director General

of Minerals, Ministry of Commerce and

allowing us to conduct field work in the

guidance with the EPMA work at UCSB.

D. Wilford and C. Knaack are thanked for

work at WSU. S. Bowring and S. Gordon

their help and support with the Sm-Nd

are thanked for help in the field during

initial sample collection with the second

author. We further thank A. El-Shazly,

C. Spencer, and an anonymous reviewer

comments. This research was supported

by an ExxonMobil/Geological Society

of America graduate student grant to J.

(USA) grants EAR-1250522 and EAR-

1650407 to M. Rioux, National Science

Foundation (USA) grant EAR-2120931 to

J. M. Garber, the University of California

at Santa Barbara, and The Pennsylvania

M. Garber, National Science Foundation

for constructive and detailed reviews,

as well as J. Walters for additional

Industry of the Sultanate of Oman for

Sultanate of Oman and facilitating its

success. G. Seward is thanked for his

and provided incisive and thoughtful

Agard, P., Jolivet, L., Vrielynck, B., Burov, E., & Monié, P. (2007). Plate acceleration: The obduction trigger? Earth and Planetary Science Letters, 258(3), 428–441. https://doi.org/10.1016/j.epsl.2007.04.002

Agard, P., Plunder, A., Angiboust, S., Bonnet, G., & Ruh, J. (2018). The subduction plate interface: Rock record and mechanical coupling (from long to short timescales). *Lithos*, 320–321, 537–566. https://doi.org/10.1016/j.lithos.2018.09.029

Agard, P., Searle, M. P., Alsop, G. I., & Dubacq, B. (2010). Crustal stacking and expulsion tectonics during continental subduction: P-T deformation constraints from Oman. *Tectonics*, 29(5), https://doi.org/10.1029/2010TC002669

Agard, P., & Vitale-Brovarone, A. (2013). Thermal regime of continental subduction: The record from exhumed HP–LT terranes (New Caledonia, Oman, Corsica). *Tectonophysics*, 601, 206–215. https://doi.org/10.1016/j.tecto.2013.05.011

Agard, P., Yamato, P., Soret, M., Prigent, C., Guillot, S., Plunder, A., et al. (2016). Plate interface rheological switches during subduction infancy: Control on slab penetration and metamorphic sole formation. *Earth and Planetary Science Letters*, 451, 208–220. https://doi.org/10.1016/j.epsl.2016.06.054

Ambrose, T. K., Waters, D. J., Searle, M. P., Gopon, P., & Forshaw, J. B. (2021). Burial, accretion, and exhumation of the metamorphic sole of the Oman-UAE ophiolite. *Tectonics*, 40(4), e2020TC006392. https://doi.org/10.1029/2020TC006392

Angiboust, S., Agard, P., Jolivet, L., & Beyssac, O. (2009). The Zermatt-Saas ophiolite: The largest (60-km wide) and deepest (c. 70–80 km) continuous slice of oceanic lithosphere detached from a subduction zone? *Terra Nova*, 21(3), 171–180. https://doi.org/10.1111/j.1365-3121.2009.00870.x Angiboust, S., Langdon, R., Agard, P., Waters, D., & Chopin, C. (2012). Eclogitization of the Monviso ophiolite (W. Alps) and implications on subduction dynamics. *Journal of Metamorphic Geology*, 30(1), 37–61. https://doi.org/10.1111/j.1525-1314.2011.00951.x

Angiolini, L., Balini, M., Garzanti, E., Nicora, A., & Tintori, A. (2003). Gondwanan deglaciation and opening of Neotethys: The Al Khlata and Saiwan Formations of Interior Oman. *Palaeogeography, Palaeoclimatology, Palaeoecology*, 196(1), 99–123. https://doi.org/10.1016/S0031-0182(03)00315-8

Bloch, E., & Ganguly, J. (2015). 176Lu–176Hf geochronology of garnet II: Numerical simulations of the development of garnet—whole-rock 176Lu–176Hf isochrons and a new method for constraining the thermal history of metamorphic rocks. *Contributions to Mineralogy and Petrology*, 169(2), 14. https://doi.org/10.1007/s00410-015-1115-x

Bouvier, A., Vervoort, J. D., & Patchett, P. J. (2008). The Lu–Hf and Sm–Nd isotopic composition of CHUR: Constraints from unequilibrated chondrites and implications for the bulk composition of terrestrial planets. *Earth and Planetary Science Letters*, 273(1), 48–57. https://doi.org/10.1016/j.epsl.2008.06.010

Bowring, S. A., Grotzinger, J. P., Condon, D. J., Ramezani, J., Newall, M. J., & Allen, P. A. (2007). Geochronologic constraints on the chronostratigraphic framework of the Neoproterozoic Huqf Supergroup, Sultanate of Oman. *American Journal of Science*, 307(10), 1097–1145. https://doi.org/10.2475/10.2007.01

Carlson, W. D. (2011). Porphyroblast crystallization: Linking processes, kinetics, and microstructures. *International Geology Review*, 53(3–4), 406–445. https://doi.org/10.1080/00206814.2010.496184

Chauvet, F., Dumont, T., & Basile, C. (2009). Structures and timing of Permian rifting in the central Oman Mountains (Saih Hatat). *Tectonophysics*, 475(3), 563–574. https://doi.org/10.1016/j.tecto.2009.07.008

GARBER ET AL.

State University.



- Chen, R.-X., Zheng, Y.-F., & Xie, L. (2010). Metamorphic growth and recrystallization of zircon: Distinction by simultaneous in-situ analyses of trace elements, U-Th-Pb and Lu-Hf isotopes in zircons from eclogite-facies rocks in the Sulu orogen. *Lithos*, 114(1-2), 132–154. https://doi.org/10.1016/j.lithos.2009.08.006
- Cherniak, D. J. (2000). Pb diffusion in rutile. Contributions to Mineralogy and Petrology, 139(2), 198–207. https://doi.org/10.1007/PL00007671
  Cowan, R. J., Searle, M. P., & Waters, D. J. (2014). Structure of the metamorphic sole to the Oman Ophiolite, Sumeini Window and Wadi Tayyin:
  Implications for ophiolite obduction processes. Geological Society, London, Special Publications, 392(1), 155–175. https://doi.org/10.1144/sp392.8
- Dewey, J. F., & Casey, J. F. (2013). The sole of an ophiolite: The Ordovician Bay of Islands Complex, Newfoundland. *Journal of the Geological Society*, 170(5), 715–722. https://doi.org/10.1144/jgs2013-017
- Dodson, M. H. (1973). Closure temperature in cooling geochronological and petrological systems. Contributions to Mineralogy and Petrology, 40(3), 259–274. https://doi.org/10.1007/BF00373790
- Duretz, T., Agard, P., Yamato, P., Ducassou, C., Burov, E. B., & Gerya, T. V. (2016). Thermo-mechanical modeling of the obduction process based on the Oman Ophiolite case. *Gondwana Research*, 32(Supplement C), 1–10. https://doi.org/10.1016/j.gr.2015.02.002
- El-Shazly, A. E.-D., Coleman, R. G., & Liou, J. G. (1990). Eclogites and Blueschists from Northeastern Oman: Petrology and P-T evolution. Journal of Petrology, 31(3), 629–666. https://doi.org/10.1093/petrology/31.3.629
- El-Shazly, A. E.-D. K. (2001). Are pressures for blueschists and eclogites overestimated? The case from NE Oman. *Lithos*, 56(2–3), 231–264. https://doi.org/10.1016/S0024-4937(00)00050-5
- El-Shazly, A. K., Bröcker, M., Hacker, B., & Calvert, A. (2001). Formation and exhumation of blueschists and eclogites from NE Oman: New perspectives from Rb–Sr and 40Ar/39Ar dating. *Journal of Metamorphic Geology*, 19(3), 233–248. https://doi.org/10.1046/j.1525-1314.2001.00309.x
- El-Shazly, A. K., & Coleman, R. G. (1990). Metamorphism in the Oman Mountains in relation to the Semail ophiolite emplacement. Geological Society, London, Special Publications, 49(1), 473–493. https://doi.org/10.1144/gsl.sp.1992.049.01.30
- El-Shazly, A. K., & Lanphere, M. A. (1992). Two high-pressure metamorphic events in NE Oman: Evidence from 40Ar/39Ar dating and petrological data. *The Journal of Geology*, 100(6), 731–751. https://doi.org/10.1086/629625
- El-Shazly, A. K., & Liou, J. G. (1991). Glaucophane chloritoid-bearing assemblages from NE Oman: Petrologic significance and a petrogenetic grid for high P metapelites. *Contributions to Mineralogy and Petrology*, 107(2), 180–201. https://doi.org/10.1007/BF00310706
- El-Shazly, A. K., Worthing, M. A., & Liou, J. G. (1997). Interlayered Eclogites, Blueschists and Epidote Amphibolites from NE Oman: A record of Protolith compositional control and limited fluid infiltration. *Journal of Petrology*, 38(11), 1461–1487. https://doi.org/10.1093/petroj/38.11.1461
- Ferry, J. M., & Watson, E. B. (2007). New thermodynamic models and revised calibrations for the Ti-in-zircon and Zr-in-rutile thermometers. Contributions to Mineralogy and Petrology, 154(4), 429–437. https://doi.org/10.1007/s00410-007-0201-0
- Fournier, M., Lepvrier, C., Razin, P., & Jolivet, L. (2006). Late Cretaceous to Paleogene post-obduction extension and subsequent Neogene compression in the Oman Mountains. *GeoArabia*, 11(4), 17–40. https://doi.org/10.2113/geoarabia110417
- Garber, J. M., Rioux, M., Kylander-Clark, A. R. C., Hacker, B. R., Vervoort, J. D., & Searle, M. P. (2020). Petrochronology of Wadi Tayin metamorphic sole metasediment, With Implications for the Thermal and Tectonic Evolution of the Samail Ophiolite (Oman/UAE). *Tectonics*, 39(12), e2020TC006135. https://doi.org/10.1029/2020TC006135
- Garber, J. M., Smye, A. J., Feineman, M. D., Kylander-Clark, A. R. C., & Matthews, S. (2020). Decoupling of zircon U-Pb and trace-element systematics driven by U diffusion in eclogite-facies zircon (Monviso meta-ophiolite, W. Alps). Contributions to Mineralogy and Petrology, 175(6), 55. https://doi.org/10.1007/s00410-020-01692-2
- Gauthiez-Putallaz, L., Rubatto, D., & Hermann, J. (2016). Dating prograde fluid pulses during subduction by in situ U–Pb and oxygen isotope analysis. Contributions to Mineralogy and Petrology, 171(2), 15. https://doi.org/10.1007/s00410-015-1226-4
- Glennie, K. W., Boeuf, M. G., Hughes-Clarke, M. H. W., Moody-Stuart, M., Pilaar, W. G., & Reinhardt, B. M. (1973). Late Cretaceous nappes in the Oman mountains and their geologic evolution. AAPG Bulletin, 57, 5–27. https://doi.org/10.1306/819a4240-16c5-11d7-8645000102c1865d
- Glodny, J., Kühn, A., & Austrheim, H. (2008). Diffusion versus recrystallization processes in Rb–Sr geochronology: Isotopic relics in eclogite facies rocks, Western Gneiss Region, Norway, *Geochimica et Cosmochimica Acta*, 72(2), 506–525, https://doi.org/10.1016/j.gca.2007.10.021
- Goffé, B., Michard, A., Kienast, J. R., & Le Mer, O. (1988). A case of obduction-related high-pressure, low-temperature metamorphism in upper crustal nappes, Arabian continental margin, Oman: P-T paths and kinematic interpretation. *Tectonophysics*, 151(1), 363–386. https://doi.org/10.1016/0040-1951(88)90253-3
- Goscombe, B., Foster, D. A., Gray, D., Kelsey, D., & Wade, B. (2020). Metamorphic response within different subduction–obduction settings preserved on the NE Arabian margin. *Gondwana Research*, 83, 298–371. https://doi.org/10.1016/j.gr.2020.02.002
- Gray, D. R., & Gregory, R. T. (2000). Implications of the structure of the Wadi Tayin metamorphic sole, the Ibra-Dasir block of the Samail ophiolite, and the Saih Hatat window for late stage extensional ophiolite emplacement, Oman. Marine Geophysical Research, 21(3), 211–227. https://doi.org/10.1023/a:1026772717865
- Gray, D. R., Gregory, R. T., Armstrong, R. A., Richards, I. J., & Miller, J. M. (2005). Age and stratigraphic relationships of structurally deepest level rocks, Oman Mountains: U/Pb SHRIMP evidence for late carboniferous neotethys rifting. The Journal of Geology, 113(6), 611–626. https://doi.org/10.1086/449325
- Gray, D. R., Gregory, R. T., & Miller, J. M. (2005). Comment on "Structural evolution, metamorphism and restoration of the Arabian continental margin, Saih Hatat region, Oman Mountains" by M.P. Searle et al. *Journal of Structural Geology*, 27(2), 371–374. https://doi.org/10.1016/j. jsg.2004.07.002
- Gray, D. R., Hand, M., Mawby, J., Armstrong, R. A., Miller, J. M., & Gregory, R. T. (2004). Sm-Nd and Zircon U-Pb ages from garnet-bearing eclogites, NE Oman: Constraints on High-P metamorphism. Earth and Planetary Science Letters, 222(2), 407–422. https://doi.org/10.1016/j.epsl.2004.03.016
- Gray, D. R., Miller, J. M., Foster, D. A., & Gregory, R. T. (2004). Transition from subduction- to exhumation-related fabrics in glaucophane-bearing eclogites, Oman: Evidence from relative fabric chronology and 40Ar/39Ar ages. *Tectonophysics*, 389(1), 35–64. https://doi.org/10.1016/j.tecto.2004.06.016
- Gregory, R. T., Gray, D. R., & Miller, J. (1998). Tectonics of the Arabian margin associated with the formation and exhumation of high-pressure rocks, Sultanate of Oman. *Tectonics*, 17(5), 657–670. https://doi.org/10.1029/98tc02206
- Haase, K. M., Freund, S., Koepke, J., Hauff, F., & Erdmann, M. (2015). Melts of sediments in the mantle wedge of the Oman ophiolite. *Geology*, 43(4), 275–278. https://doi.org/10.1130/G36451.1
- Hacker, B. R., & Mosenfelder, J. L. (1996). Metamorphism and deformation along the emplacement thrust of the Samail ophiolite, Oman. Earth and Planetary Science Letters, 144(3-4), 435-451. https://doi.org/10.1016/s0012-821x(96)00186-0
- Hu, J., & Gurnis, M. (2020). Subduction duration and slab dip. Geochemistry, Geophysics, Geosystems, 21(4), e2019GC008862. https://doi.org/10.1029/2019gc008862

GARBER ET AL. 23 of 26



- Johnson, T. A., Vervoort, J. D., Ramsey, M. J., Aleinikoff, J. N., & Southworth, S. (2018). Constraints on the timing and duration of orogenic events by combined Lu–Hf and Sm–Nd geochronology: An example from the Grenville orogeny. Earth and Planetary Science Letters, 501, 152–164. https://doi.org/10.1016/j.epsl.2018.08.030
- Johnston, S. M., Hacker, B. R., & Andersen, T. B. (2007). Exhuming Norwegian ultrahigh-pressure rocks: Overprinting extensional structures and the role of the Nordfjord-Sogn Detachment Zone. *Tectonics*, 26(5). https://doi.org/10.1029/2005TC001933
- Jolivet, L., Goffé, B., Bousquet, R., Oberhänsli, R., & Michard, A. (1998). Detachments in high-pressure mountain belts, Tethyan examples. Earth and Planetary Science Letters, 160(1), 31–47. https://doi.org/10.1016/S0012-821X(98)00079-X
- Kylander-Clark, A. R. C., Hacker, B. R., & Cottle, J. M. (2013). Laser-ablation split-stream ICP petrochronology. *Chemical Geology*, 345, 99–112. https://doi.org/10.1016/j.chemgeo.2013.02.019
- Kylander-Clark, A. R. C., Hacker, B. R., Johnson, C. M., Beard, B. L., & Mahlen, N. J. (2009). Slow subduction of a thick ultrahigh-pressure terrane. *Tectonics*, 28(2). https://doi.org/10.1029/2007TC002251
- Kylander-Clark, A. R. C., Hacker, B. R., & Mattinson, C. G. (2012). Size and exhumation rate of ultrahigh-pressure terranes linked to orogenic stage. Earth and Planetary Science Letters. 321–322, 115–120. https://doi.org/10.1016/j.epsl.2011.12.036
- Kylander-Clark, A. R. C., Hacker, B. R., & Mattinson, J. M. (2008). Slow exhumation of UHP terranes: Titanite and rutile ages of the Western Gneiss Region, Norway. Earth and Planetary Science Letters, 272(3–4), 531–540. https://doi.org/10.1016/j.epsl.2008.05.019
- Lapen, T. J., Johnson, C. M., Baumgartner, L. P., Mahlen, N. J., Beard, B. L., & Amato, J. M. (2003). Burial rates during prograde metamorphism of an ultra-high-pressure terrane: An example from Lago di Cignana, western Alps, Italy. Earth and Planetary Science Letters, 215(1), 57–72. https://doi.org/10.1016/S0012-821X(03)00455-2
- Le Metour, J., Rabu, D., Tegyey, M., Bechennec, F., Beurrier, M., & Villey, M. (1986). Le métamorphisme régional crétacé de faciès éclogites-schistes bleus sur la bordure omanaise de la plate-forme arabe: Conséquence d'une tectogenèse précoce anté-obduction. Comptes Rendus de l'Académie des Sciences, Série II, 302, 905–910.
- Le Métour, J., Rabu, D., Tegyey, M., Béchennec, F., Beurrier, M., & Villey, M. (1990). Subduction and obduction: Two stages in the Eo-Alpine tectonometamorphic evolution of the Oman Mountains. Geological Society, London, Special Publications, 49(1), 327–339. https://doi.org/10.1144/gsl.sp.1992.049.01.20
- Lippard, S. J. (1983). Cretaceous high pressure metamorphism in NE Oman and its relationship to subduction and ophiolite nappe emplacement. Journal of the Geological Society, 140(1), 97–104. https://doi.org/10.1144/gsjgs.140.1.0097
- Mann, A., & Hanna, S. S. (1990). The tectonic evolution of pre-Permian rocks, Central and Southeastern Oman Mountains. Geological Society, London, Special Publications, 49(1), 307–325. https://doi.org/10.1144/gsl.sp.1992.049.01.19
- Massonne, H.-J., Opitz, J., Theye, T., & Nasir, S. (2013). Evolution of a very deeply subducted metasediment from As Sifah, northeastern coast of Oman. Lithos, 156(Supplement C), 171–185. https://doi.org/10.1016/j.lithos.2012.11.009
- McDonough, W. F., & Sun, S. S. (1995). The composition of the earth. Chemical Geology, 120(3), 223–253. https://doi. org/10.1016/0009-2541(94)00140-4
- Mercolli, I., Briner, A. P., Frei, R., Schönberg, R., Nägler, T. F., Kramers, J., et al. (2006). Lithostratigraphy and geochronology of the Neoproterozoic crystalline basement of Salalah, Dhofar, Sultanate of Oman. *Precambrian Research*, 145(3), 182–206. https://doi.org/10.1016/j.precamres.2005.12.002
- Michard, A. (1983). Les nappes de Mascate (Oman), rampe épicontinentale d'obduction à faciès schiste bleu, et la dualité apparente des ophiolites omanaises, Sciences Géologiques, bulletins et mémoires, 36, 3–16. https://doi.org/10.3406/sgeol.1983.1624
- Michard, A., Boudier, F., & Goffé, B. (1991). Obduction versus subduction and collision in the Oman case and other tethyan Settings, paper presented at Ophiolite Genesis and evolution of the oceanic lithosphere. Springer.
- Michard, A., Goffé, B., Saddiqi, O., Oberhänsli, R., & Wendt, A. S. (1994). Late cretaceous exhumation of the oman blueschists and eclogites: A two-stage extensional mechanism. Terra Nova, 6(4), 404–413. https://doi.org/10.1111/j.1365-3121.1994.tb00514.x
- Miller, J. M., Gray, D. R., & Gregory, R. T. (1998). Exhumation of high-pressure rocks in northeastern Oman. *Geology*, 26(3), 235–238. https://doi.org/10.1130/0091-7613(1998)026<0235:eohpri>2.3.co;2
- Miller, J. M., Gray, D. R., & Gregory, R. T. (2002). Geometry and significance of internal windows and regional isoclinal folds in northeast Saih Hatat, Sultanate of Oman. *Journal of Structural Geology*, 24(2), 359–386. https://doi.org/10.1016/S0191-8141(01)00061-X
- Miller, J. M., Gregory, R. T., Gray, D. R., & Foster, D. A. (1999). Geological and geochronological constraints on the exhumation of a high-pressure metamorphic terrane, Oman. Geological Society, London, Special Publications, 154(1), 241–260. https://doi.org/10.1144/gsl. sp.1999.154.01.11
- Montigny, R., Le Mer, O., Thuizat, R., & Whitechurch, H. (1988). K-Ar and Ar study of metamorphic rocks associated with the Oman ophiolite: Tectonic implications. *Tectonophysics*, 151(1–4), 345–362. https://doi.org/10.1016/0040-1951(88)90252-1
- Nicolas, A., Boudier, F., Ildefonse, B., & Ball, E. (2000). Accretion of Oman and United Arab Emirates ophiolite Discussion of a new structural map. *Marine Geophysical Research*, 21(3), 147–180. https://doi.org/10.1023/a:1026769727917
- Pattison, D. R. M., & Tinkham, D. K. (2009). Interplay between equilibrium and kinetics in prograde metamorphism of pelites: An example from the Nelson aureole, British Columbia. *Journal of Metamorphic Geology*, 27(4), 249–279. https://doi.org/10.1111/j.1525-1314.2009.00816.x
- Poupeau, G., Saddiqi, O., Michard, A., Goffé, B., & Oberhänsli, R. (1998). Late thermal evolution of the Oman Mountains subophiolitic windows: Apatite fission-track thermochronology. *Geology*, 26(12), 1139–1142, https://doi.org/10.1130/0091-7613(1998)026<1139:lteoto>2.3.co;2
- Rioux, M., Benoit, M., Amri, I., Ceuleneer, G., Garber, J. M., Searle, M., et al. (2021). The origin of felsic intrusions within the mantle section of the Samail ophiolite: Geochemical evidence for three distinct mixing and fractionation trends. *Journal of Geophysical Research: Solid Earth*, 126(5), e2020JB020760. https://doi.org/10.1029/2020JB020760
- Rioux, M., Bowring, S., Kelemen, P., Gordon, S., Miller, R., & Dudás, F. (2013). Tectonic development of the Samail ophiolite: High-precision U-Pb zircon geochronology and Sm-Nd isotopic constraints on crustal growth and emplacement. *Journal of Geophysical Research: Solid Earth*, 118(5), 2085–2101. https://doi.org/10.1002/jgrb.50139
- Rioux, M., Bowring, S. A., Kelemen, P. B., Gordon, S., Dudás, F., & Miller, R. (2012). Rapid crustal accretion and magma assimilation in the Oman-U.A.E. ophiolite: High precision U-Pb zircon geochronology of the gabbroic crust. *Journal of Geophysical Research*, 117. https://doi. org/10.1029/2012JB009273
- Rioux, M., Garber, J., Bauer, A., Bowring, S., Searle, M., Kelemen, P., et al. (2016). Synchronous formation of the metamorphic sole and igneous crust of the Semail ophiolite: New constraints on the tectonic evolution during ophiolite formation from high-precision U-Pb zircon geochronology. Earth and Planetary Science Letters, 451, 185–195. https://doi.org/10.1016/j.epsl.2016.06.051
- Rioux, M., Garber, J. M., Searle, M., Kelemen, P., Miyashita, S., Adachi, Y., et al. (2021). High-Precision U-Pb Zircon dating of late magmatism in the Samail ophiolite: A record of subduction initiation. *Journal of Geophysical Research: Solid Earth*, 126(5), e2020JB020758. https://doi.org/10.1029/2020JB020758

GARBER ET AL. 24 of 26



- Robertson, A. H. F. (1987). Upper cretaceous muti formation: Transition of a Mesozoic nate platform to a foreland basin in the Oman Mountains. Sedimentology, 34(6), 1123–1142. https://doi.org/10.1111/j.1365-3091.1987.tb00596.x
- Rollinson, H. (2009). New models for the genesis of plagiogranites in the Oman ophiolite. Lithos, 112(3-4), 603-614. https://doi.org/10.1016/j. lithos.2009.06.006
- Rollinson, H. (2015). Slab and sediment melting during subduction initiation: Granitoid dykes from the mantle section of the Oman ophiolite. Contributions to Mineralogy and Petrology, 170(3), 1–20. https://doi.org/10.1007/s00410-015-1177-9
- Rubatto, D. (2017). Zircon: The metamorphic mineral. Reviews in Mineralogy and Geochemistry, 83(1), 261–295. https://doi.org/10.2138/rmg.2017.83.9
- Rubatto, D., & Angiboust, S. (2015). Oxygen isotope record of oceanic and high-pressure metasomatism: A P-T-time-fluid path for the Monviso eclogites (Italy). Contributions to Mineralogy and Petrology, 170(5), 44. https://doi.org/10.1007/s00410-015-1198-4
- Rubatto, D., & Hermann, J. (2003). Zircon formation during fluid circulation in eclogites (Monviso, Western Alps): Implications for Zr and Hf budget in subduction zones. Geochimica et Cosmochimica Acta, 67(12), 2173–2187. https://doi.org/10.1016/S0016-7037(02)01321-2
- Rubatto, D., & Hermann, J. (2007). Experimental zircon/melt and zircon/garnet trace element partitioning and implications for the geochronology of crustal rocks. *Chemical Geology*, 241(1–2), 38–61. https://doi.org/10.1016/j.chemgeo.2007.01.027
- Rubatto, D., & Hermann, J. r. (2001). Exhumation as fast as subduction? *Geology*, 29(1), 3–6. https://doi.org/10.1130/0091-7613(2001)029<0 003:eafas>2.0.co:2
- Rubatto, D., Regis, D., Hermann, J., Boston, K., Engi, M., Beltrando, M., et al. (2011). Yo-yo subduction recorded by accessory minerals in the Italian Western Alps. *Nature Geoscience*, 4, 338–342. https://doi.org/10.1038/ngeo1124
- Saddiqi, O., Michard, A., Goffe, B., Poupeau, G. R., & Oberhänsli, R. (2006). Fission-track thermochronology of the Oman Mountains continental windows, and current problems of tectonic interpretation. Bulletin de la Societe Geologique de France, 177(3), 127–134. https://doi.org/10.2113/gssgfbull.177.3.127
- Scherer, E. E., Cameron, K. L., & Blichert-Toft, J. (2000). Lu-Hf garnet geochronology: Closure temperature relative to the Sm-Nd system and the effects of trace mineral inclusions, *Geochimica et Cosmochimica Acta*, 64(19), 3413–3432, https://doi.org/10.1016/S0016-7037(00)00440-3
- Searle, M. P. (2007). Structural geometry, style and timing of deformation in the Hawasina Window, Al Jabal al Akhdar and Saih Hatat culminations, Oman Mountains. GeoArabia, 12(2), 99–130. https://doi.org/10.2113/geoarabia120299
- Searle, M. P., & Cox, J. (1999). Tectonic setting, origin, and obduction of the Oman ophiolite. Geological Society of America Bulletin, 111(1), 104–122. https://doi.org/10.1130/0016-7606(1999)111<0104:tsoaoo>2.3.co;2
- Searle, M. P., & Cox, J. (2002). Subduction zone metamorphism during formation and emplacement of the Semail ophiolite in the Oman Mountains. Geological Magazine, 139(3), 241–255. https://doi.org/10.1017/s0016756802006532
- Searle, M. P., Warren, C. J., Waters, D. J., & Parrish, R. R. (2004). Structural evolution, metamorphism and restoration of the Arabian continental margin, Saih Hatat region, Oman Mountains. *Journal of Structural Geology*, 26(3), 451–473. https://doi.org/10.1016/j.jsg.2003.08.005
- Searle, M. P., Warren, C. J., Waters, D. J., & Parrish, R. R. (2005). Reply to: Comment by Gray, Gregory and Miller on "Structural evolution, metamorphism and restoration of the Arabian continental margin, Saih Hatat region, Oman Mountains". *Journal of Structural Geology*, 27(2), 375–377. https://doi.org/10.1016/j.jsg.2004.07.003
- Searle, M. P., Waters, D. J., Martin, H. N., & Rex, D. C. (1994). Structure and metamorphism of blueschist-eclogite facies rocks from the north-eastern Oman Mountains. *Journal of the Geological Society*, 151(3), 555–576. https://doi.org/10.1144/gsjgs.151.3.0555
- Sherlock, S., Kelley, S., Inger, S., Harris, N., & Okay, A. (1999). 40Ar-39Ar and Rb-Sr geochronology of high-pressure metamorphism and exhumation history of the Tavsanli Zone, NW Turkey. *Contributions to Mineralogy and Petrology*, 137(1), 46–58. https://doi.org/10.1007/PI.00013777
- Smye, A. J., Marsh, J. H., Vermeesch, P., Garber, J. M., & Stockli, D. F. (2018). Applications and limitations of U-Pb thermochronology to middle and lower crustal thermal histories. *Chemical Geology*, 494, 1–18. https://doi.org/10.1016/j.chemgeo.2018.07.003
- Smye, A. J., Warren, C. J., & Bickle, M. J. (2013). The signature of devolatisation: Extraneous 40Ar systematics in high-pressure metamorphic rocks. Geochimica et Cosmochimica Acta, 113, 94–112. https://doi.org/10.1016/j.gca.2013.03.018
- Soret, M., Agard, P., Dubacq, B., Plunder, A., & Yamato, P. (2017). Petrological evidence for stepwise accretion of metamorphic soles during subduction infancy (Semail ophiolite, Oman and UAE). *Journal of Metamorphic Geology*, 35, 1051–1080. https://doi.org/10.1111/jmg.12267
- Spencer, C. J., Cavosie, A. J., Raub, T. D., Rollinson, H., Jeon, H., Searle, M. P., et al. (2017). Evidence for melting mud in Earth's mantle from extreme oxygen isotope signatures in zircon. *Geology*, 45(11), 975–978. https://doi.org/10.1130/g39402.1
- Stern, R. J., & Johnson, P. (2010). Continental lithosphere of the Arabian Plate: A geologic, petrologic, and geophysical synthesis. *Earth-Science Reviews*, 101(1), 29–67. https://doi.org/10.1016/j.earscirev.2010.01.002
- Štípská, P., Powell, R., Hacker, B. R., Holder, R., & Kylander-Clark, A. R. C. (2016). Uncoupled U/Pb and REE response in zircon during the transformation of eclogite to mafic and intermediate granulite (Blanský les, Bohemian Massif). *Journal of Metamorphic Geology*, 34(6), 551–572. https://doi.org/10.1111/jmg.12193
- Taylor, R. J. M., Clark, C., Harley, S. L., Kylander-Clark, A. R. C., Hacker, B. R., & Kinny, P. D. (2017). Interpreting granulite facies events through rare earth element partitioning arrays. *Journal of Metamorphic Geology*, 35(7), 759–775. https://doi.org/10.1111/jmg.12254
- Tomkins, H. S., Powell, R., & Ellis, D. J. (2007). The pressure dependence of the zirconium-in-rutile thermometer. *Journal of Metamorphic Geology*, 25(6), 703–713. https://doi.org/10.1111/j.1525-1314.2007.00724.x
- Villa, I. M. (2010). Disequilibrium textures versus equilibrium modelling: Geochronology at the crossroads. Geological Society, London, Special Publications, 332(1), 1–15. https://doi.org/10.1144/sp332.1
- Vitale Brovarone, A., & Agard, P. (2013). True metamorphic isograds or tectonically sliced metamorphic sequence? New high-spatial resolution petrological data for the New Caledonia case study. *Contributions to Mineralogy and Petrology*, 166(2), 451–469. https://doi.org/10.1007/s00410-013-0885-2
- Vitale-Brovarone, A., Groppo, C., Hetényi, G., Compagnoni, R., & Malavieille, J. (2011). Coexistence of lawsonite-bearing eclogite and blueschist: Phase equilibria modelling of Alpine Corsica metabasalts and petrological evolution of subducting slabs. *Journal of Metamorphic Geology*, 29(5), 583–600. https://doi.org/10.1111/j.1525-1314.2011.00931.x
- Warren, C., Parrish, R., Waters, D., & Searle, M. (2005). Dating the geologic history of Oman's Semail ophiolite: Insights from U-Pb geochronology. Contributions to Mineralogy and Petrology, 150(4), 403–422. https://doi.org/10.1007/s00410-005-0028-5
- Warren, C. J., & Miller, J. M. (2007). Structural and stratigraphic controls on the origin and tectonic history of a subducted continental margin, Oman. *Journal of Structural Geology*, 29(3), 541–558. https://doi.org/10.1016/j.jsg.2006.10.006
- Warren, C. J., Parrish, R. R., Searle, M. P., & Waters, D. J. (2003). Dating the subduction of the Arabian continental margin beneath the Semail ophiolite, Oman. *Geology*, 31(10), 889–892. https://doi.org/10.1130/g19666.1
- Warren, C. J., Sherlock, S. C., & Kelley, S. P. (2011). Interpreting high-pressure phengite 40Ar/39Ar laserprobe ages: An example from Saih Hatat, NE Oman. Contributions to Mineralogy and Petrology, 161(6), 991–1009. https://doi.org/10.1007/s00410-010-0576-1

GARBER ET AL. 25 of 26



- Warren, C. J., & Waters, D. J. (2006). Oxidized eclogites and garnet-blueschists from Oman: P-T path modelling in the NCFMASHO system. Journal of Metamorphic Geology, 24(9), 783–802. https://doi.org/10.1111/j.1525-1314.2006.00668.x
- Wendt, A. S., D'Arco, P., Goffé, B., & Oberhänsli, R. (1993). Radial cracks around α-quartz inclusions in almandine: Constraints on the metamorphic history of the Oman mountains. *Earth and Planetary Science Letters*, 114(4), 449–461. https://doi.org/10.1016/0012-821X(93)90075-K Wendt, I., & Carl, C. (1991). The statistical distribution of the mean squared weighted deviation. *Chemical Geology*, 86(4), 275–285. https://doi.org/10.1016/0168-9622(91)90010-t
- Yamato, P., Agard, P., GoffÉ, B., De Andrade, V., Vidal, O., & Jolivet, L. (2007). New, high-precision P-T estimates for Oman blueschists: Implications for obduction, nappe stacking and exhumation processes. *Journal of Metamorphic Geology*, 25(6), 657–682. https://doi.org/10.1111/j.1525-1314.2007.00722.x
- Young, D. J. (2017). Structure of the (ultra)high-pressure Western Gneiss Region, Norway: Imbrication during Caledonian continental margin subduction. GSA Bulletin, 130(5–6), 926–940. https://doi.org/10.1130/b31764.1
- Young, D. J., Hacker, B. R., Andersen, T. B., & Gans, P. B. (2011). Structure and 40Ar/39Ar thermochronology of an ultrahigh-pressure transition in western Norway. *Journal of the Geological Society*, 168(4), 887–898. https://doi.org/10.1144/0016-76492010-075
- Young, D. J., & Kylander-Clark, A. R. C. (2015). Does continental crust transform during eclogite facies metamorphism? *Journal of Metamorphic Geology*, 33(4), 331–357. https://doi.org/10.1111/jmg.12123

# **References From The Supporting Information**

- Begemann, F., Ludwig, K. R., Lugmair, G. W., Min, K., Nyquist, L. E., Patchett, P. J., et al. (2001). Call for an improved set of decay constants for geochronological use. *Geochimica et Cosmochimica Acta*, 65(1), 111–121. https://doi.org/10.1016/S0016-7037(00)00512-3
- Camacho, A. (1997). An isotopic study of deep-crustal processes: Musgrave Block (pp. 504). Australian National University.
- Ewing, T. A. (2011). Hf isotope analysis and U-Pb geochronology of rutile: Technique development and application to a lower crustal section (Ivrea-Verbano Zone, Italy) (pp. 385). Australian National University.
- Jackson, S. E., Pearson, N. J., Griffin, W. L., & Belousova, E. A. (2004). The application of laser ablation-inductively coupled plasma-mass spectrometry to in situ U-Pb zircon geochronology. Chemical Geology, 211(1), 47-69. https://doi.org/10.1016/j.chemgeo.2004.06.017
- Jochum, K. P., Willbold, M., Raczek, I., Stoll, B., & Herwig, K. (2005). Chemical characterisation of the USGS reference glasses GSA-1G, GSC-1G, GSD-1G, GSE-1G, BCR-2G, BHVO-2G and BIR-1G using EPMA, ID-TIMS, ID-ICP-MS and LA-ICP-MS. Geostandards and Geoanalytical Research, 29(3), 285–302. https://doi.org/10.1111/j.1751-908X.2005.tb00901.x
- Ludwig, K. R. (2003). Isoplot 3.00: A geochronological toolkit for microsoft excel. Berkeley Geochronology Center Special Publication.
- Luvizotto, G. L., Zack, T., Meyer, H. P., Ludwig, T., Triebold, S., Kronz, A., et al. (2009). Rutile crystals as potential trace element and isotope mineral standards for microanalysis. Chemical Geology, 261(3), 346–369. https://doi.org/10.1016/j.chemgeo.2008.04.012
- Paton, C., Hellstrom, J., Paul, B., Woodhead, J., & Hergt, J. (2011). Iolite: Freeware for the visualisation and processing of mass spectrometric data. *Journal of Analytical Atomic Spectrometry*, 26(12), 2508–2518. https://doi.org/10.1039/C1JA10172B
- Pearce, N. J. G., Perkins, W. T., Westgate, J. A., Gorton, M. P., Jackson, S. E., Neal, C. R., et al. (1997). A compilation of new and published major and trace element data for NIST SRM 610 and NIST SRM 612 glass reference materials. *Geostandards Newsletter*, 21(1), 115–144. https://doi.org/10.1111/j.1751-908X.1997.tb00538.x
- Sláma, J., Košler, J., Condon, D. J., Crowley, J. L., Gerdes, A., Hanchar, J. M., et al. (2008). Plešovice zircon A new natural reference material for U–Pb and Hf isotopic microanalysis. *Chemical Geology*, 249(1), 1–35. https://doi.org/10.1016/j.chemgeo.2007.11.005
- Wiedenbeck, M., AllÉ, P., Corfu, F., Griffin, W. L., Meier, M., Oberli, F., et al. (1995). Three natural zircon standards for U-TH-PB, LU-HF, trace element and ree analyses. *Geostandards Newsletter*, 19(1), 1–23. https://doi.org/10.1111/j.1751-908X.1995.tb00147.x

GARBER ET AL. 26 of 26